AMERICAN SOCIETY FOR MICROBIOLOGY | Molecular and Cellular Biology®

RESEARCH ARTICLE

Specific Modification of Aged Proteasomes Revealed by Tag-Exchangeable Knock-In Mice

Takuya Tomita,[a] Shoshiro Hirayama,[a] Yasuyuki Sakurai,[a] Yuki Ohte,[a] Hidehito Yoshihara,[b] Yasushi Saeki,[b] Jun Hamazaki,[a] Shigeo Murata[a]

[a]Laboratory of Protein Metabolism, Graduate School of Pharmaceutical Sciences, The University of Tokyo, Tokyo, Japan
[b]Laboratory of Protein Metabolism, Tokyo Metropolitan Institute of Medical Science, Tokyo, Japan

ABSTRACT The proteasome is the proteolytic machinery at the center of regulated intracellular protein degradation and participates in various cellular processes. Maintaining the quality of the proteasome is therefore important for proper cell function. It is unclear, however, how proteasomes change over time and how aged proteasomes are disposed. Here, we show that the proteasome undergoes specific biochemical alterations as it ages. We generated Rpn11-Flag/enhanced green fluorescent protein (EGFP) tag-exchangeable knock-in mice and established a method for selective purification of old proteasomes in terms of their molecular age at the time after synthesis. The half-life of proteasomes in mouse embryonic fibroblasts isolated from these knock-in mice was about 16 h. Using this tool, we found increased association of Txnl1, Usp14, and actin with the proteasome and specific phosphorylation of Rpn3 at Ser 6 in 3-day-old proteasomes. We also identified *CSNK2A2* encoding the catalytic α' subunit of casein kinase II (CK2α') as a responsible gene that regulates the phosphorylation and turnover of old proteasomes. These findings will provide a basis for understanding the mechanism of molecular aging of the proteasome.

KEYWORDS knock-in mice, molecular aging, proteasome, protein turnover, whole-genome siRNA screen

The 26S proteasome is an enzymatic complex that mainly degrades ubiquitinated proteins (1, 2). This large protein complex is composed of a central 20S core particle (CP) capped at either or both ends by 19S regulatory particles (RPs) (3). The CP is made up of seven structurally similar α- and β-subunits (α1 to α7 and β1 to β7) and is responsible for proteolysis. The RPs consist of six ATPases (Rpt1 to Rpt6) and multiple non-ATPase subunits (Rpn1 to Rpn3, Rpn5 to Rpn13, and Rpn15) and plays essential roles in capturing ubiquitin chains, deubiquitinating, and unfolding substrates. In addition to the authentic proteasome subunits, proteasome interacting proteins (PIPs) that transiently associate with the proteasome to play auxiliary roles have been identified. For example, the proteasome assembly chaperones PAC1 to PAC4, the deubiquitinating enzymes Usp14 and Uch37, and ubiquitin receptors HHR23, and ubiquilins are well characterized (4–9). On the other hand, there still remain many PIPs whose functions are elusive, including the thioredoxin-like protein Txnl1 (10, 11).

The proteasome plays pivotal roles in various cellular events such as cell cycle, transcription, and immune response (12, 13). Recent reports have shown that senescence and diseases such as neurodegenerative diseases are associated with aberrant proteasome activity and that modulation of proteasome activity can regulate such diseases (14). It has been shown that proteasome activity declines with aging (15). Ubiquitinated misfolded proteins have been shown to accumulate in many neurodegenerative diseases, which are often associated with a decline in proteasome activity with aging (16). Downregulation of proteasome activity also triggers autoinflammatory

Citation Tomita T, Hirayama S, Sakurai Y, Ohte Y, Yoshihara H, Saeki Y, Hamazaki J, Murata S. 2019. Specific modification of aged proteasomes revealed by tag-exchangeable knock-in mice. Mol Cell Biol 39:e00426-18. https://doi.org/10.1128/MCB.00426-18.

Address correspondence to Shigeo Murata, smurata@mol.f.u-tokyo.ac.jp.

Received 28 August 2018
Returned for modification 21 September 2018
Accepted 10 October 2018
Accepted manuscript posted online 22 October 2018
Published 11 December 2018

disorder in patients with mutations in proteasome subunit genes (17–20). An artificial increase in proteasome activity leads to life span extension and concomitantly prevents neurodegeneration or confers stress resistance in *Drosophila melanogaster* and *Caenorhabditis elegans* (21–23). Therefore, uncovering the mechanism by which the quality of the proteasome is maintained is important for understanding the pathogenesis of numerous human diseases. More specifically, how the proteasome changes over time and how such changes affect proteasome activity remain unknown.

Turnover of the proteasome is one of the regulatory mechanisms of quality control of the proteasome. It is possible that damaged or unnecessary proteasomes are removed and that the regulation of the turnover of the proteasome is important for maintaining cellular homeostasis. Indeed, recent reports showed that the proteasome can be degraded by autophagy. Nitrogen starvation and proteasome inhibition induce autophagy-mediated degradation of the 26S proteasome in *Arabidopsis* and yeast (24–26), and amino acid starvation triggers autophagy that targets the 26S proteasome in mammalian cells (27). However, such autophagic degradation of the proteasome was observed in response to specific extracellular stimuli. Few studies have explored constitutive degradation of the 26S proteasome, which is likely to be well regulated, considering that the proteasome has a measurable half-life (28, 29).

To address these issues, we biochemically characterized 3-day-old proteasomes in terms of their molecular age at the time after synthesis. Using genetically engineered mice that express a subunit of the proteasome with an exchangeable tag, 3-day-old proteasomes were selectively purified. This analysis revealed differences in protein-protein interactions, posttranslational modifications, and subcellular localization between old and new proteasomes. We then identified genes that affect the turnover of proteasomes by a genome-wide small interfering RNA (siRNA) screen in human cells. As a result, we determined genes that delayed the turnover of old proteasomes.

RESULTS

Generation of Rpn11-Flag/EGFP tag-exchangeable mice and MEFs. To purify old proteasomes, we generated Rpn11-Flag/enhanced green fluorescent protein (EGFP) tag-exchangeable knock-in mice (Fig. 1A). Rpn11, which is encoded by the *Psmd14* gene, is one of the subunits of the RP. In the targeting vector, a sequence encoding a 6×His-Flag epitope was fused to the 3′ end of the last coding nucleotide in exon 12, followed by a poly(A) signal. The modified exon 12 and a *flippase recombinase target* (*FRT*)-flanked phosphoglycerate kinase (PGK)-neomycin gene cassette were flanked by two *loxP* sequences. Another modified exon 12 that was fused to an EGFP coding sequence and a poly(A) signal was placed downstream of the 3′ *loxP* so that the C-terminal tag of Rpn11 switches from 6×His-Flag to EGFP upon expression of Cre recombinase.

The targeting vector was introduced into TT2 embryonic stem (ES) cells, and successful homologous recombination of the *Psmd14* genomic region was confirmed by Southern blot analysis (Fig. 1B). The heterozygous knock-in ($Psmd14^{Flag/+}$) ES cells expressed Rpn11-Flag (Fig. 1C). Once Cre recombinase was expressed in the cells, Rpn11-EGFP was expressed, while Rpn11-Flag decreased, indicating that the *loxP*-flanked segment was excised to induce tag switching ($Psmd14^{EGFP/+}$) (Fig. 1C).

The $Psmd14^{Flag/+}$ ES cells were microinjected into eight-cell embryos of ICR mice, and the produced chimeric mice were intercrossed with C57BL/6 mice for at least five generations. Although $Psmd14^{Flag/+}$ mice were born without any gross abnormality and were fertile, the homozygous knock-in $Psmd14^{Flag/Flag}$ mice were embryonic lethal (see Table S1 in the supplemental material). To obtain $Psmd14^{EGFP/+}$ mice, we crossed $Psmd14^{Flag/+}$ mice with mice expressing Cre recombinase throughout the whole body directed by the adenovirus-derived EIIa promoter (30). Whereas $Psmd14^{Flag/Flag}$ mice showed lethality, $Psmd14^{EGFP/EGFP}$ mice were fertile and grew without any gross abnormality (Table S1). This suggests that highly charged 6×His-Flag epitope fused to Rpn11 might interfere a function of Rpn11 or the proteasome during embryonic development. EGFP fluorescence was detectable in $Psmd14^{EGFP/EGFP}$ mice, indicating that the tag

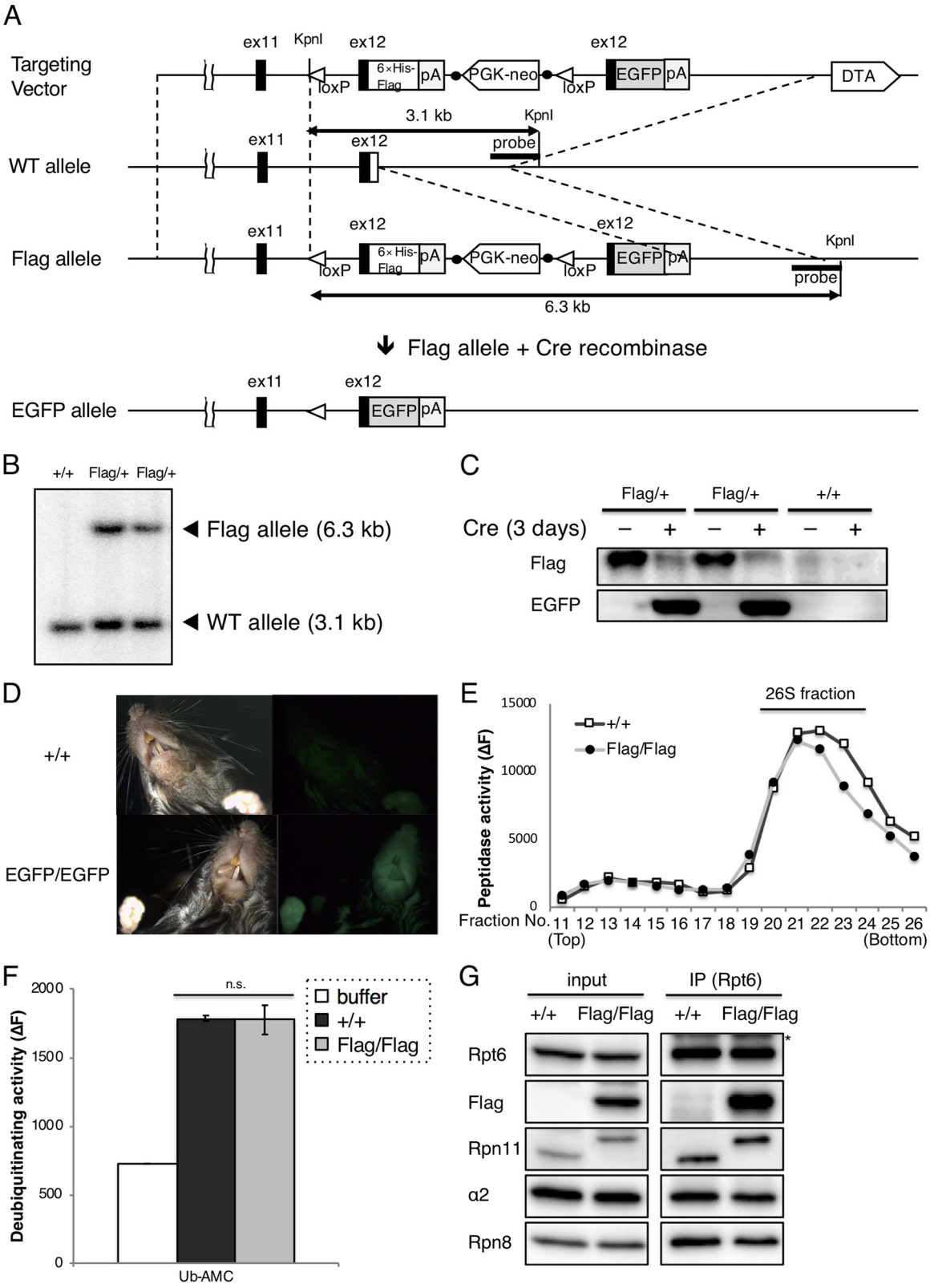

FIG 1 Generation of Rpn11-Flag/EGFP tag-exchangeable knock-in mice. (A) Schematic representation of the integration strategy for generating C-terminally tagged Flag fusion Rpn11. After Cre-mediated recombination, the *loxP*-flanked segment is excised, and the expression of Flag tag is exchanged for EGFP tag. WT, ex11, ex12, pA, PGK, DTA, and neo denote wild-type, exon 11, exon 12, polyadenylation signal, PGK promoter sequence, diphtheria toxin A, and neomycin-resistant cassette, respectively. The black dot indicates the *FRT* site. (B) Southern blot analysis of KpnI-digested genomic DNAs extracted from mouse tails. Wild-type and Flag knock-in alleles were detected as 3.1- and 6.3-kb bands, respectively. (C) Immunoblotting of embryonic stem cell extracts infected with or without

(Continued on next page)

exchange was successful in mice (Fig. 1D and Fig. S1A). We were, however, able to obtain *Psmd14*$^{Flag/Flag}$ mouse embryonic fibroblasts (MEFs) from embryonic day 13.5 (E13.5) embryos, which we will refer to as Rpn11-Flag MEFs.

To examine whether there is any loss of function of the proteasome in Rpn11-Flag MEFs compared to wild-type MEFs (*Psmd14*$^{+/+}$), we fractionated lysates of MEFs by glycerol gradient centrifugation, followed by measurement of peptidase activity of each fraction. The peptidase activities were almost identical between wild-type and Rpn11-Flag MEFs (Fig. 1E). The 26S fraction of Rpn11-Flag MEFs did not show a significant difference in the deubiquitinating activity compared to wild-type MEFs (Fig. 1F). We also verified the incorporation of Rpn11-Flag into the 26S proteasome by immunoprecipitation assay using antibodies against the RP subunit Rpt6. The composition of the proteasome containing Rpn11-Flag was similar to that of the control proteasomes, as revealed by coprecipitated proteasome subunits, β1 and Rpn8 (Fig. 1G). As observed in these experiments, we did not find any notable defects in the proteasome in Rpn11-Flag MEFs. We therefore utilized Rpn11-Flag MEFs as an alternative to *Psmd14*$^{Flag/Flag}$ mice for proteasome analysis.

To exchange the tag in Rpn11-Flag MEFs, we used retroviruses expressing Cre recombinase (Cre-retrovirus) at a high multiplicity. By infection of Cre-retrovirus, EGFP fluorescence was observed from almost all cells, suggesting that the tag exchange occurred efficiently (Fig. S1B). Thus, we successfully generated Rpn11-Flag/EGFP tag exchangeable mice and MEFs as new tools for proteasome research.

Differences in proteins interacting with old proteasomes. To establish an experimental system to purify "old" proteasomes, we first examined the half-life of the proteasome in Rpn11-Flag MEFs by the pulse-chase method. 26S proteasomes turned over slowly with a half-life of about 16 h, which was almost the same as the doubling time of Rpn11-Flag MEFs (Fig. 2A and Fig. S2A). However, we hypothesized that the proteasome undergoes biochemical alterations as it ages and expected to identify factors associated with turnover mechanism of old proteasomes. We found that 3-day-old proteasomes constituted no more than 5% of the total proteasomes (Fig. 2A), suggesting that characteristics of old proteasomes should be observable with a 3-day chase. Therefore, 3-day cultures of Rpn11-Flag MEFs after infection with Cre-retrovirus allowed us to purify old proteasomes that are produced more than 3 days ago by immunoprecipitating with anti-Flag antibody, whereas proteasomes incorporating Rpn11-EGFP are relatively "new" proteasomes produced within 72 h, assuming that Rpn11 does not dissociate from the RP after the RP is assembled (Fig. 2B).

Rpn11-Flag MEFs were infected with Cre-retrovirus and, 3 days later, old proteasomes were purified using anti-Flag–agarose beads. We did not purify new proteasomes by anti-EGFP antibody for comparison between new and old proteasomes because the difference in tags and antibodies used for purification might yield false differences that would make it difficult to identify true differences. Instead, "total" proteasomes were purified from Rpn11-Flag MEFs infected with retroviruses that do not express Cre to compare with the old proteasomes (Fig. 2B).

Subunit composition of 3-day-old proteasomes did not show obvious alterations compared to total proteasomes, as shown by immunoblot analysis of the CP subunit β3 and the RP subunits Rpt6 and Rpn8 and by silver staining of each immunoprecipitate following SDS-PAGE (Fig. 3A and B). Note that Rpn11-EGFP, which was newly synthesized after the expression of Cre recombinase, was slightly detected in the old proteasome complex (Fig. 3A). This was probably due to formation of 26S proteasome that

FIG 1 Legend (Continued)
adenovirus expressing Cre recombinase. (D) Gross appearance of *Psmd14*$^{+/+}$ and *Psmd14*$^{EGFP/EGFP}$ mice. Bright-field and fluorescence images of 3-week-old mice are shown. (E) Lysates from wild-type and Rpn11-Flag MEFs were fractionated by 8 to 32% glycerol gradient centrifugation. An aliquot of each fraction was used for an assay of chymotryptic activity of the proteasome using Suc-LLVY-AMC as a substrate. (F) The 26S fractions in panel E were subjected to the assay of the deubiquitinating activity using ubiquitin-AMC as a substrate. The data represent means ± the standard deviations (SD) from triplicate experiments. n.s., not significant. (G) Lysates from wild-type and Rpn11-Flag MEFs were subjected to immunoprecipitation with anti-Rpt6 antibodies, followed by immunoblotting with the indicated antibodies. The asterisk denotes IgG. The data are representative of three independent experiments.

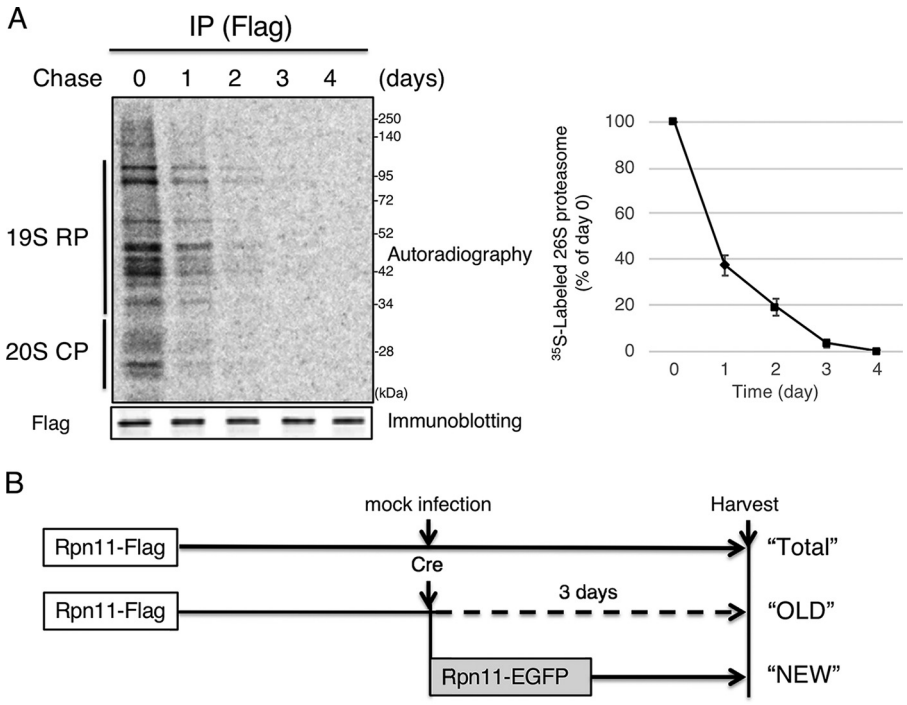

FIG 2 Development of strategies to purify old proteasomes. (A) Rpn11-Flag MEFs were radiolabeled and chased for the indicated time. Lysates were immunoprecipitated with anti-Flag antibodies and subjected to SDS-PAGE, followed by autoradiography and immunoblotting. Values represent means ± the SD of the relative band intensities (normalized to Flag) obtained from three independent experiments. (B) The experimental scheme for the purification of the total, old, and new proteasomes using Rpn11-Flag MEFs.

has an old RP containing Rpn11-Flag on one side and a new RP containing Rpn11-EGFP on the other, suggesting some plasticity of interaction between CP and RP in cells. However, the contamination of Rpn11-EGFP in the proteasome purified with anti-Flag beads is small enough to consider that the proteasome purified via Rpn11-Flag are representative of old proteasomes.

We also examined the amount of several proteasome-interacting proteins bound to old proteasomes. While the deubiquitinating enzyme Uch37, as well as the ubiquitin receptor HHR23b, was recruited almost equally to total and old proteasomes, the thioredoxin-like protein Txnl1, the deubiquitinating enzyme Usp14, and the cytoskeletal protein actin showed increased interactions with old proteasomes (Fig. 3A). In contrast, the association of ubiquitinated proteins with old proteasomes was reduced (Fig. 3A). This may be due to the increased interaction with Usp14, which might deubiquitinate substrates on old proteasomes.

Increased oxidation status of old proteasomes. Previous studies suggested that several posttranslational modifications may influence enzymatic activities of the proteasome (31–35). Therefore, we examined whether old proteasomes underwent specific modifications. Since carbonylation is commonly used as an indicator for protein damage caused by oxidative stress (36), protein carbonyls of the total and 3-day-old proteasomes were visualized by OxyBlot (Fig. 3C). The bands corresponding to the size of old RP subunits showed approximately 30% increased levels of carbonylation, suggesting that the proteasome RP or proteins copurified with the proteasome are subjected to oxidative stress damage as it ages.

Enhanced phosphorylation of Rpn3 at serine 6 in old proteasomes. We also analyzed the phosphorylation status of old proteasomes because it is an influential posttranslational modification that regulates proteasome function, as well as various intracellular signals (31–35). Purified total and 3-day-old proteasomes were examined by SDS-PAGE containing Phos-tag acrylamide, in which phosphorylated proteins are

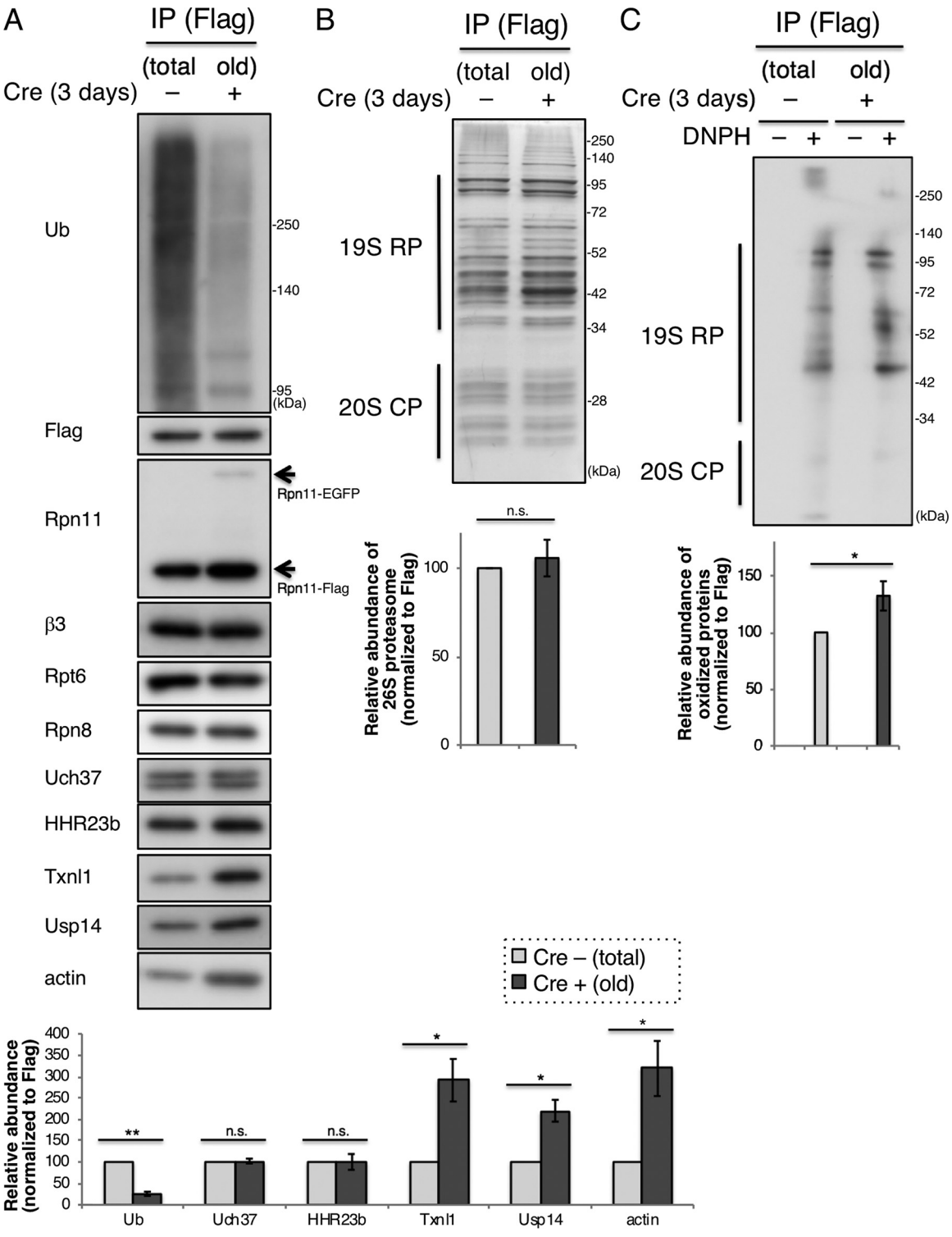

FIG 3 Purification of old proteasomes. (A) Rpn11-Flag MEFs were infected with control or Cre recombinase-expressing retrovirus, and 3 days later the cells were harvested. Lysates were immunoprecipitated with anti-Flag antibodies, followed by Flag peptide elution. The amounts of proteasomes loaded were adjusted for the protein level of Rpn11-Flag and subjected to immunoblotting with the indicated antibodies. Values represent means ± the SD of the relative band intensities (normalized to Flag) obtained from three independent experiments. n.s., not significant; *, $P < 0.05$. (B) Proteasomes containing Rpn11-Flag purified as for panel A were subjected to SDS-PAGE and silver stained for protein. Values represent means ± the SD of the relative band intensities (normalized to Flag in panel A) obtained from three independent experiments. n.s., not significant. (C) An OxyBlot protein oxidation detection kit was used for the immunoblot detection of carbonyl groups introduced into proteins of the purified proteasomes shown in panel A. The carbonyl groups in the protein side chains were derivatized by reaction with 2,4-dinitrophenylhydrazine (DNPH). Values represent means ± the SD of the relative band intensities (normalized to Flag in panel A) obtained from three independent experiments. *, $P < 0.05$.

detected by retarded mobility shift (37). Although most of the old RP subunits did not show any notable band shifts by Phos-tag acrylamide, the mobility of a fraction of Rpn3 in old proteasomes was specifically retarded, indicating the phosphorylation of old Rpn3 (Fig. 4A). We expected to detect the phosphorylation of other subunits, as reported previously (31–35), but they were not detectable, suggesting that the stoichiometry of phosphorylated subunits other than Rpn3 is low in Rpn11-Flag MEFs.

To determine the phosphorylation site, the bands corresponding to the total and the old Rpn3 were excised and analyzed by mass spectrometry. While unphosphorylated peptide 202-209 (ALDLVAAK) was detected in almost equal amounts between total and old Rpn3, phosphorylated peptide 1-8 (MKQEGpSAR) was almost exclusively detected in Rpn3 from 3-day-old proteasomes (Fig. 4B and C). The amount of phosphorylated Rpn3 at serine 6 of total proteasomes was less than 5% of that of 3-day-old proteasomes, supporting successful purification of old proteasomes (Fig. 2A).

The N terminus of Rpn3 is thought to be located on the surface of the proteasome complex (38, 39), and Rpn3 at serine 6 is highly conserved only in mammals (Fig. 4D). To confirm the phosphorylation of Rpn3 in old proteasomes, we raised antibodies that specifically recognize either the phosphorylated or unphosphorylated forms of Rpn3 at serine 6 (anti-pSer6-Rpn3 and anti-unphosphorylated-Rpn3 antibodies, respectively). The anti-pSer6-Rpn3 antibodies specifically recognized the band corresponding to phosphorylated Rpn3, whereas anti-unphosphorylated-Rpn3 antibodies detected only the band which was not affected by Phos-tag acrylamide (Fig. 4E). This demonstrates that the old Rpn3 at serine 6 was certainly phosphorylated.

Enhanced deubiquitinating activity and normal proteolytic activity of old proteasomes. Since old proteasomes showed alterations in the amount of some specific interacting proteins, as well as oxidation and phosphorylation states, we examined whether these differences influenced the enzymatic activities of old proteasomes. The enzymatic activities of the proteasome were assessed by *in vitro* experiments using model substrates.

Deubiquitinating activity was measured using the model substrate ubiquitin-AMC. Old proteasomes exhibited increased deubiquitinating activity, which is probably due to the elevated association of Usp14 with old proteasomes (Fig. 5A; also Fig. 3A).

We next examined ATP-dependent protease activity by *in vitro* degradation assay against two substrates. The degradation rates of ornithine decarboxylase (ODC) and ubiquitinated inhibitor of apotosis 1 (Ub-cIAP1), which are degraded by the proteasome in ubiquitin-independent and -dependent manners, respectively (40, 41), were comparable between the total and 3-day-old proteasomes (Fig. 5B).

The 26S proteasome exhibits three different peptidase activities: chymotrypsin-like, trypsin-like, and caspase-like activities. We measured these catalytic activities for hydrolysis of Suc-LLVY-AMC, Boc-LRR-AMC, and Z-LLE-AMC, respectively (42), and found that peptidase activities of old proteasomes were not compromised (Fig. 5C). Thus, protein hydrolyzing activities of old proteasomes were almost comparable to that of the total proteasomes, at least when estimated by *in vitro* experiments.

Decreased nuclear localization of old proteasomes. We further examined the localization of old proteasomes because changes in protein-protein interaction and posttranslational modification often affect subcellular localization of modified proteins. Rpn11-Flag MEFs infected with Cre-retrovirus were immunostained with anti-Flag antibodies to visualize old proteasomes in a microscopy analysis (Fig. 5D). New proteasomes were observed by Rpn11-EGFP fluorescence. The viral titer used in this assay was much lower than in other experiments in order to detect all old, new, and total proteasomes in the same visual field. The fluorescence of Rpn11-EGFP was mainly detected in the nucleus. In contrast, old proteasomes stained against Rpn11-Flag in Rpn11-EGFP-positive cells were mainly detected in the cytosol. The total proteasomes indicated by anti-Flag immunofluorescence in Rpn11-EGFP-negative cells showed higher fluorescence intensity in the nucleus than in the cytosol.

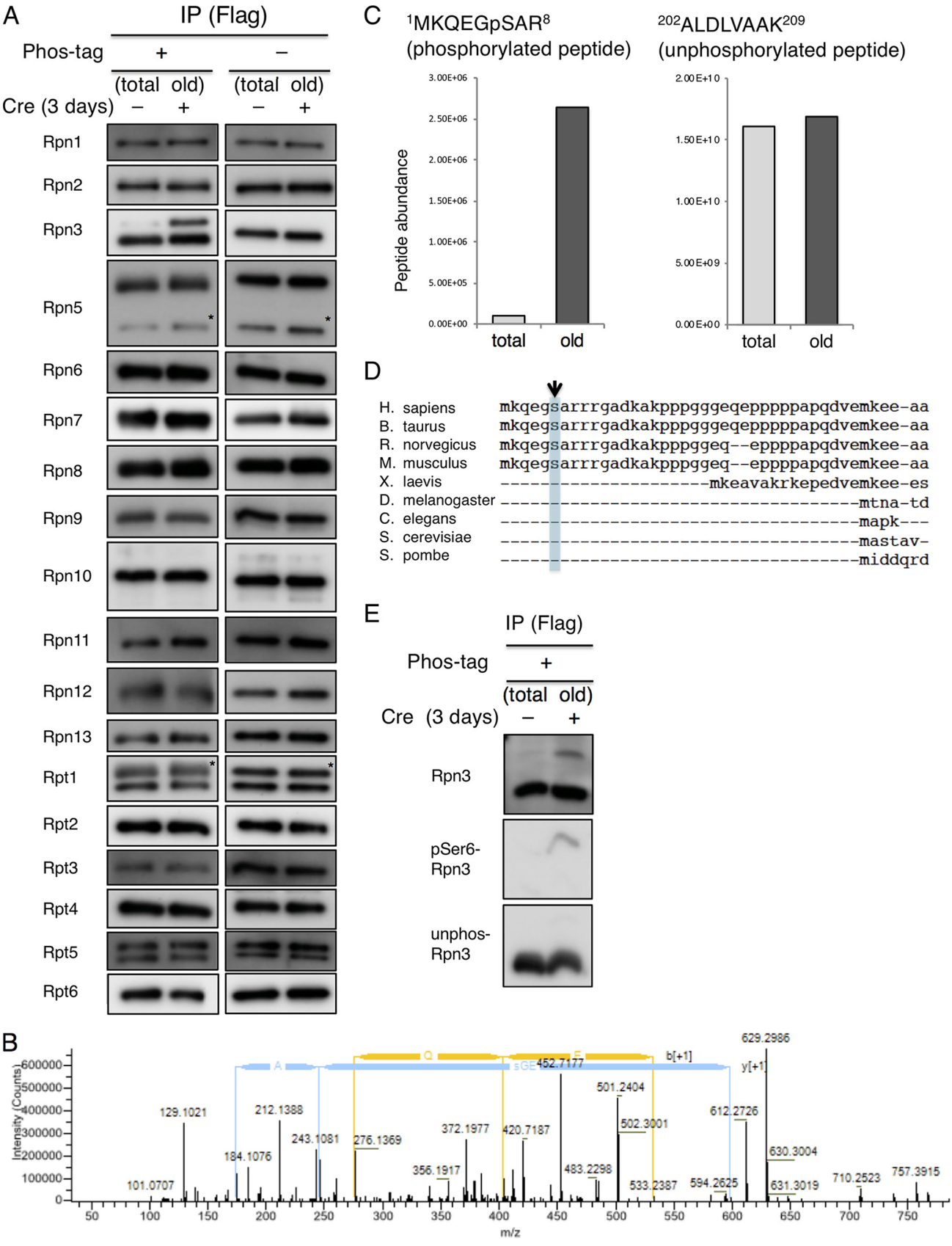

FIG 4 Phosphorylation of old proteasomes. (A) Rpn11-Flag MEFs were infected with control or Cre recombinase-expressing retrovirus, and 3 days later the cells were harvested. Lysates were immunoprecipitated with anti-Flag antibodies, followed by Flag peptide elution. The samples were normalized by the

(Continued on next page)

This finding was supported by cell fractionation analysis (Fig. 5E). After Cre expression, the decrease in Rpn11-Flag was greater in the nucleus than in the cytosol. On the other hand, the expression of new proteasomes observed by Rpn11-EGFP was higher in the nucleus than the cytosol. These results suggest that subcellular localization of the proteasome changes, depending on whether it is newly produced or aged.

Generation of Rpn11-Halo knock-in cells that enables visualization of old and new proteasomes. Although old proteasomes were biochemically characterized, the mechanism of their degradation remains elusive, with the exception of stress-induced autophagic degradation (24–27). To investigate the mechanism of constitutive degradation of the proteasome, we performed a genome-wide siRNA screen to identify genes that affect the turnover of proteasomes. We used HaloTag labeling technology by which HaloTag conjugated proteins were labeled with fluorescent chemical ligands (43). Similar to the construction of Rpn11-Flag/EGFP tag-exchangeable knock-in mice, a sequence encoding HaloTag was fused to the 3′ end of the last coding nucleotide in exon 12 of *PSMD14* encoding Rpn11, followed by a poly(A) signal and a PGK-puromycin expression cassette for the selection of positive cells in which homologous recombination was successful (Fig. 6A). We generated Rpn11-Halo knock-in cell lines using the CRISPR/Cas9 system to monitor the turnover of proteasomes in HeLa cells (44). The expression and incorporation of Rpn11-Halo into the proteasome complex, as well as wild-type Rpn11, were confirmed by immunoprecipitation with antibodies against the RP subunit Rpt6 (Fig. 6B). To ascertain the integrity of proteasomes in the knock-in cells, lysates of parental cells and Rpn11-Halo knock-in cells were fractionated by glycerol gradient centrifugation. The peptidase activities of proteasomes in each fraction showed no significant differences between wild-type and Rpn11-Halo knock-in cells, suggesting that the function of proteasomes in the Rpn11-Halo knock-in cells was normal (Fig. 6C).

To visualize old and new proteasomes, a pulse-chase labeling experiment was performed (Fig. 6D). Rpn11-Halo knock-in cells were treated with Oregon Green (OG) HaloTag ligand to label preexisting Rpn11-Halo, followed by treatment with blocking ligand to mask HaloTag that did not react with OG ligand. One, two, or three days after treatment with OG and blocking ligands, the cells were treated with tetramethylrhodamine (TMR) HaloTag ligand to detect newly synthesized Rpn11-Halo before cell harvest. The fluorescence intensity of OG-labeled Rpn11-Halo that represents the amount of old proteasomes decreased, while the fluorescence intensity of TMR-labeled newly synthesized Rpn11-Halo increased as the chase period was extended (Fig. 6E), showing successful discrimination between old and new proteasomes by pulse-chase HaloTag labeling. The half-life of Rpn11-Halo, about 24 h, was again almost the same with the doubling time of Rpn11-Halo HeLa cells (Fig. 6E and Fig. S2B).

Genome-wide siRNA screen for identification of genes that affect the turnover of proteasomes. Using Rpn11-Halo knock-in cells and proteasome labeling, a genome-wide siRNA screen was performed to identify genes that affect the turnover of proteasomes. Rpn11-Halo knock-in cells were treated with OG ligands to label old proteasomes, followed by blocking ligand treatment, and then plated on 384-well plates to transfect a pooled siRNA library (a pool of four unique siRNA targets per gene) (Fig. S3A). After incubation for 64 h, the cells were treated with TMR ligands to label new proteasomes that were synthesized in the last 64 h. The cells were then fixed and stained with DAPI (4′,6′-diamidino-2-phenylindole). The number of the cells and the fluorescence intensities of OG and TMR per cell were quantified by high-content

FIG 4 Legend (Continued)
protein level of Rpn11-Flag, analyzed by SDS-PAGE (10% [wt/vol] polyacrylamide containing 0 or 50 μM Phos-tag), and subjected to immunoblotting with the indicated antibodies. The asterisks denote nonspecific bands. The data are representative of three independent experiments. (B) Mass spectrometric analysis of the tryptic phosphopeptide MKQEGpSAR from Rpn3 in 3-day-old proteasomes. (C) Relative quantification of MKQEGpSAR and ALDLVAAK peptides from Rpn3 in the total and 3-day-old proteasomes. (D) Alignment of Rpn3 N-terminal sequences. Residues that correspond to the possible phosphorylation site serine 6 are shaded. (E) The proteasomes purified as for Fig. 3A were analyzed by SDS-PAGE (10% [wt/vol] polyacrylamide containing 50 μM Phos-tag), followed by immunoblotting with the indicated antibodies.

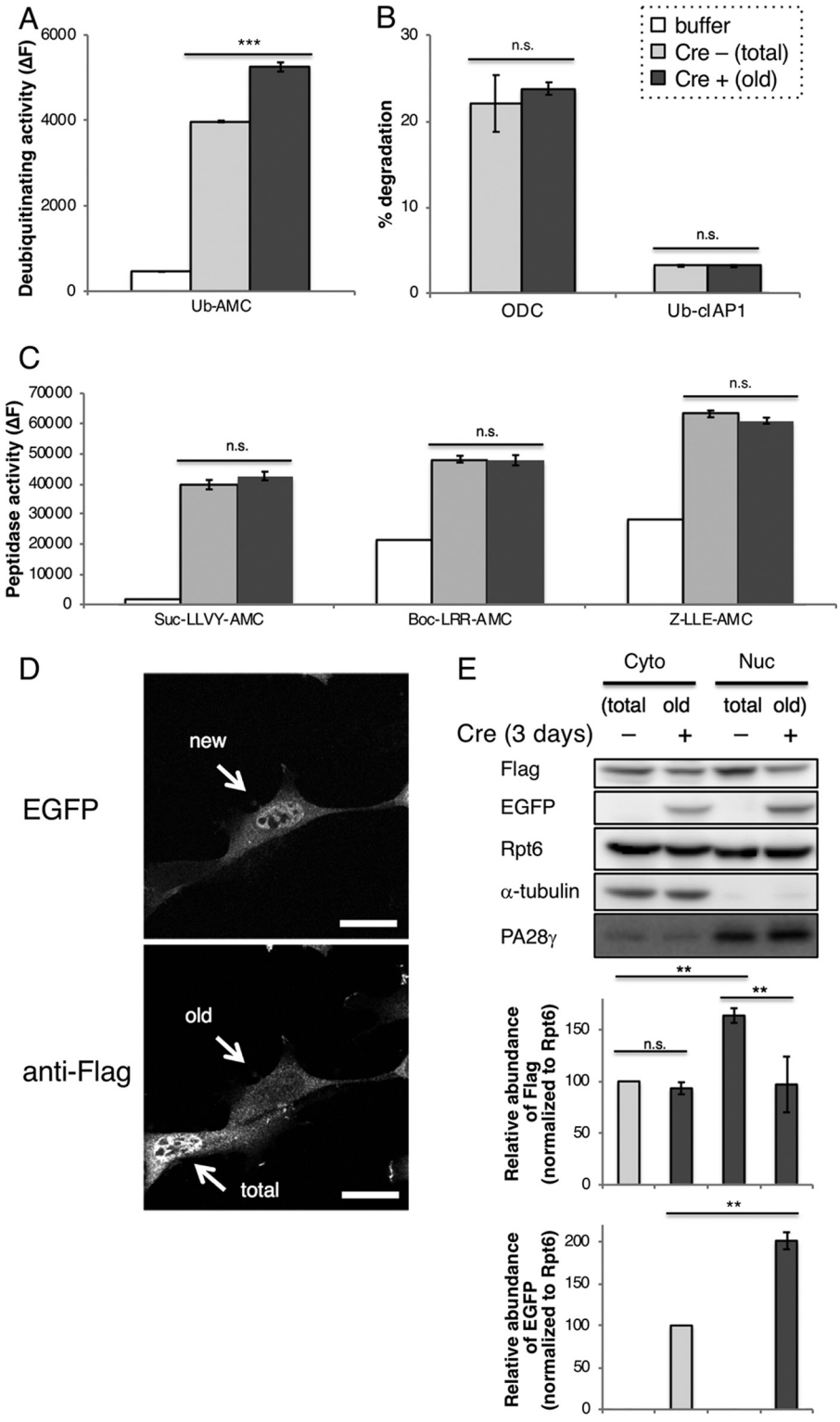

FIG 5 Biochemical characterization of old proteasomes. (A) The deubiquitinating activities of 26S proteasomes purified as for Fig. 3A were measured using ubiquitin-AMC as a substrate. The data represent means ± the SD from triplicate experiments. ***, $P < 0.001$. (B) Ubiquitin-independent and -dependent protease activities of proteasomes. The proteasomes purified as for Fig. 3A were subjected to *in vitro* protein degradation assay. Antizyme-dependent degradation of ^{35}S-labeled ODC and ubiquitin-dependent degradation of ^{35}S-labeled polyubiquitinated cIAP1 were measured. The data represent means ± the SD from triplicate experiments. n.s., not significant. (C) Peptidase activities of the proteasome. The purified proteasomes shown in Fig. 3A were subjected to *in vitro* degradation assay using Suc-LLVY-AMC, Boc-LRR-AMC, and Z-LLE-AMC as the substrates to assess the chymotrypsin-like, trypsin-like, and caspase-like activities, respectively. The data represent means ±

(Continued on next page)

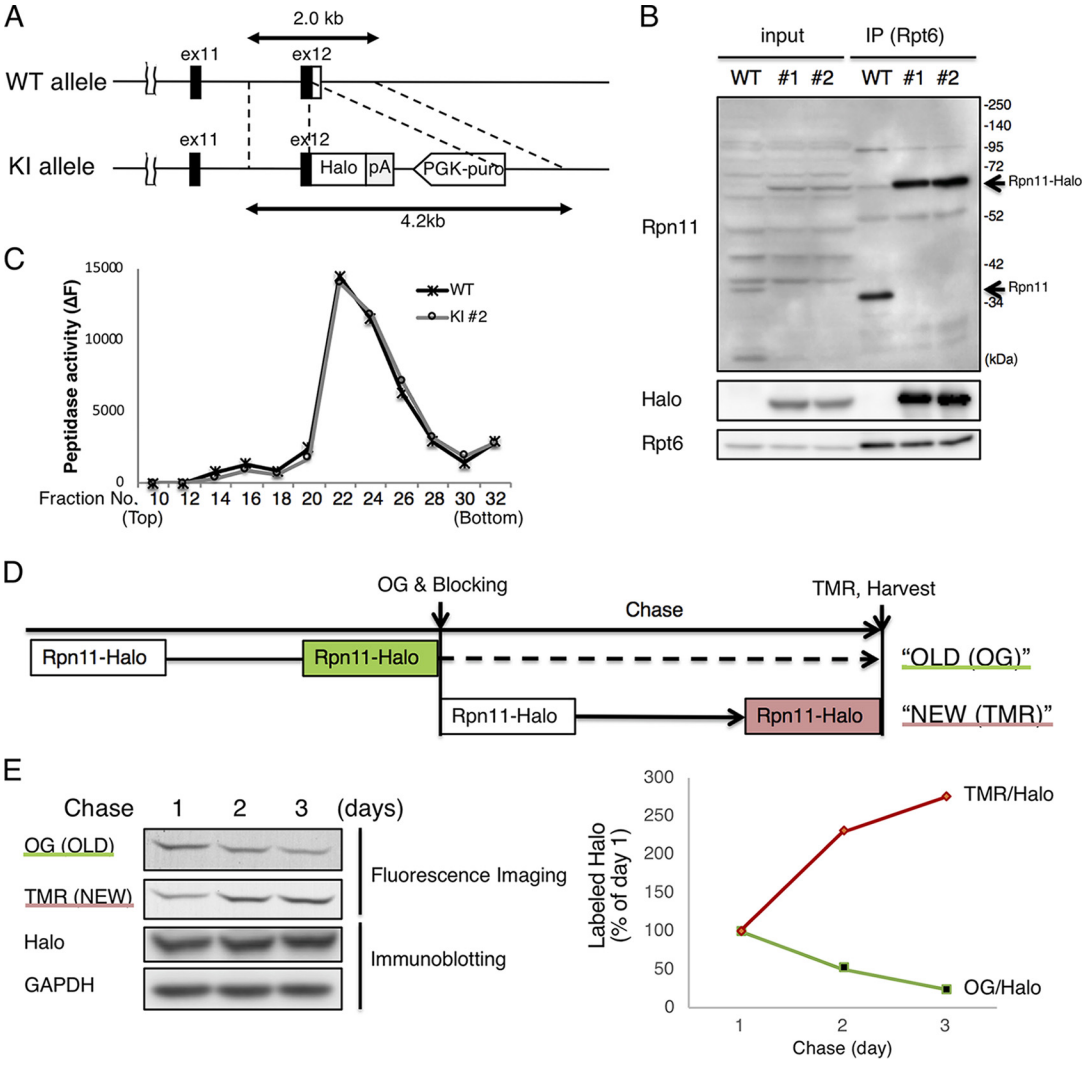

FIG 6 CRISPR/Cas9-mediated endogenous tagging of Rpn11 with HaloTag in HeLa cells. (A) Schematic representation of the integration strategy for generating C-terminally tagged HaloTag fusion Rpn11 proteins expressed from endogenous locus in HeLa cell. (B) Lysates from wild-type and Rpn11-Halo knock-in cells (clones 1 and 2) were subjected to immunoprecipitation with anti-Rpt6 antibodies, followed by immunoblotting with the indicated antibodies. (C) Lysates from wild-type and Rpn11-Halo knock-in cells (clone 2) were fractionated by 8 to 32% glycerol gradient centrifugation. An aliquot of each fraction was used for an assay of chymotryptic activity of the proteasome using Suc-LLVY-AMC as a substrate. (D) Schematic view of labeling old and new proteasomes using Rpn11-Halo knock-in cells. (E) Rpn11-Halo knock-in cells (clone 2) were treated with OG ligands and subsequently subjected to the blocking ligand. After the indicated time, the cells were then treated with TMR ligand. Harvested cells were stored at −80°C until they were lysed. Lysates were subjected to fluorescence imaging and immunoblotting. GAPDH served as a loading control. Values represent the relative band intensities (normalized to Halo).

microscopy and automated image analysis. siRNA targeting *PSMD14* (Rpn11), which drastically decreased fluorescence intensity of TMR, served as a positive control for labeling of Rpn11-Halo (Fig. S3B).

To identify siRNA targets that delay the turnover of proteasomes, we focused on genes whose knockdown caused high fluorescence intensity of OG, which represents

FIG 5 Legend (Continued)
the SD from triplicate experiments. n.s., not significant. (D) Representative images of Rpn11-Flag MEFs infected with retrovirus expressing Cre recombinase at a low multiplicity for 3 days. The cells were immunostained with anti-Flag antibodies. Scale bars, 25 μm. (E) Rpn11-Flag MEFs were infected with control or Cre recombinase-expressing retrovirus, and 3 days later the cells were harvested. Lysates were fractionated into cytosols and nuclei by digitonin treatment. α-Tubulin and PA28γ served as loading controls for the cytosolic and nuclear fractions, respectively. Values represent means $\pm$ the SD of the relative band intensities (normalized to Rpt6) obtained from three independent experiments. n.s., not significant; **, $P < 0.01$.

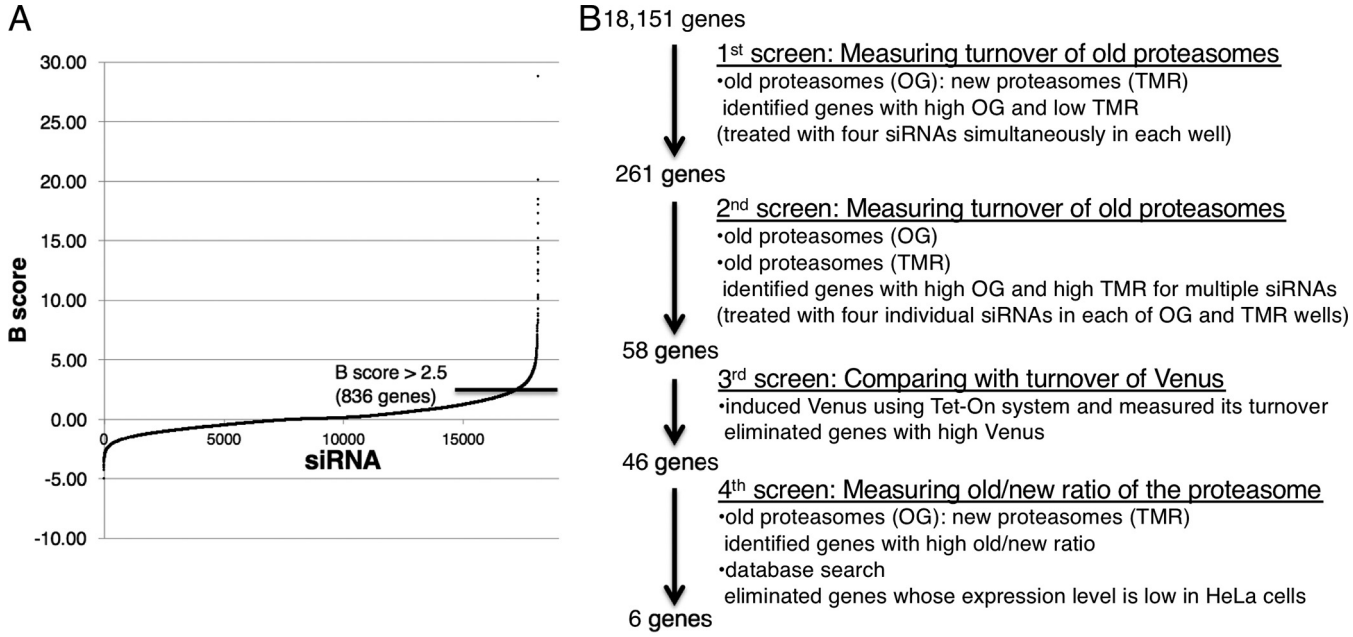

C

	1st screen	2nd screen	3rd screen	4th screen	Gene function (UniProt/NCBI database)
	B score	Positive siRNA number		old/new ratio (vs negative control siRNA)	
ARCN1	8.18	3	2	1.91	Golgi-to-ER transport
CSNK2A2	4.05	2	2	1.51	α' catalytic subunit of CK2
EPOR	4.51	2	2	1.23	erythropoietin receptor
NR1H2	4.52	2	2	1.59	liver X nuclear receptor β
SAYSD1	4.09	2	2	1.55	uncharacterized
SORL1	4.03	2	2	1.23	endocytic receptor

FIG 7 Primary screen for the identification of genes that affect the turnover of proteasomes. (A) B scores of OG in the primary screen. The data are ordered from lowest to highest. The black line represents the cutoff value for positive hits. The list of B scores for all samples in the primary screen are available in Data Set S1. (B) Graphical representation of the genome-wide siRNA screen. (C) List of the final six hit genes and scores in each assay throughout the screening process. NCBI, National Center for Biotechnology Information; ER, endoplasmic reticulum; CK2, casein kinase II.

the amount of old proteasomes. From 836 genes that marked the top 5% B score of OG fluorescence intensity (B score $>$ 2.5) in the primary screen, we eliminated false-positives such as detachment of cells from the assay plates by visual inspection (Fig. 7A and B). We also eliminated wells showing high TMR intensity that represent enhanced proteasome expression rather than delay in degradation of the proteasome and wells with very small cell counts due to poor cell growth (Fig. 7B). As a result, 261 genes were chosen for the second screen where we used four individual siRNAs for each target gene and performed Rpn11-Halo labeling by treating cells with either OG or TMR before siRNA transfection (Fig. 7B). The intensity of OG or TMR was measured for each siRNA for the amounts of old proteasomes, and we chose 58 genes that had a high score (B score $>$ 1.5 among the 261 genes) in more than two of four siRNA knockdowns in both OG and TMR labeling experiments for the third screen (Fig. 7B). In the third screen, we selected 46 genes whose knockdown specifically affected the decrease in old proteasomes by comparison with the decrease in Venus as a reference fluorescent protein that was expressed by the Tet-On induction system (Fig. S3C). These candidate

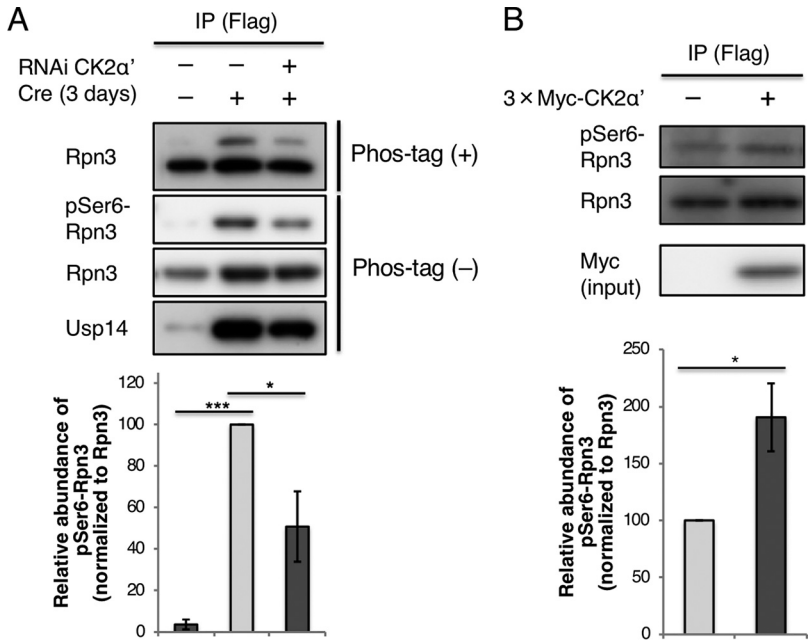

FIG 8 Phosphorylation of Rpn3 is regulated by CK2α'. (A) Transfection of negative control or CK2α' siRNA for 6 days in Rpn11-Flag MEFs, followed by infection with control or Cre recombinase-expressing retrovirus for 3 days. Lysates were immunoprecipitated with anti-Flag antibodies, followed by Flag peptide elution. The samples were analyzed by SDS-PAGE (10% [wt/vol] polyacrylamide containing 50 μM Phos-tag) and subjected to immunoblotting with the indicated antibodies. Values represent means $\pm$ the SD of the relative band intensities (normalized to Rpn3 in the absence of Phos-tag) obtained from three independent experiments. ***, $P < 0.001$; *, $P < 0.05$. (B) 3×Myc-CK2α' was overexpressed in Rpn11-Flag MEFs for 48 h. Lysates were immunoprecipitated with anti-Flag antibodies. The samples were analyzed by SDS-PAGE (10% [wt/vol] polyacrylamide containing 50 μM Phos-tag) and subjected to immunoblotting with the indicated antibodies. Values represent means $\pm$ the SD of the relative band intensities (normalized to Rpn3 in the absence of Phos-tag) obtained from three independent experiments. *, $P < 0.05$.

genes were further evaluated for whether the siRNAs increased the ratio of old to new proteasomes (old/new) by flow cytometry. Finally, we eliminated genes whose expression level is low in HeLa cells with database searches (45). Consequently, we obtained six genes whose knockdown markedly delayed the turnover of proteasomes (Fig. 7B and C).

Identification of genes responsible for the phosphorylation of Rpn3. Of the final hits, we focused on *CSNK2A2*, which encodes the catalytic α' subunit of casein kinase II (CK2α'), because phosphorylation of the proteasome is known to affect the function of the proteasome (31–35) and because we observed specific phosphorylation of Rpn3 subunit in old proteasomes (Fig. 4). Reverse transcription-PCR (RT-PCR) confirmed successful knockdown of human and mouse CK2α' (*CSNK2A2* and *Csnk2a2*, respectively) by an siRNA that targeted a sequence common to both human and mouse (Fig. S4A and B).

To examine whether CK2α' is involved in phosphorylation of Rpn3 of old proteasomes, CK2α' siRNA was transfected before expression of Cre recombinase in Rpn11-Flag MEFs (Fig. 8A). Old proteasomes (Cre+) increased the interaction with Usp14 and included pSer6-Rpn3, consistent with the results shown in Fig. 3 and 4. Knockdown of CK2α' reduced pSer6-Rpn3 in old proteasomes, suggesting that CK2α' is involved in the phosphorylation of Rpn3. A decrease in pSer6-Rpn3 was also observed in CK2α' knockdown HEK293T cells (Fig. S4C). Conversely, the overexpression of CK2α', which is known to form a constitutively active kinase complex (46), enhanced the phosphorylation of Rpn3 in Rpn11-Flag MEFs and HEK293T cells (Fig. 8B and Fig. S4D). These results indicate that CK2α' is involved in the phosphorylation of Rpn3. Considering that CK2α' regulates the turnover of old proteasomes by specifically phosphorylating Rpn3,

it is possible that phosphorylation of Rpn3 regulates proteasome turnover, although this remains to be proved.

DISCUSSION

In this study, we generated Rpn11-Flag/EGFP tag-exchangeable knock-in mice for purification and visualization of the proteasome. Using this new tool, we established methods for quantification and purification of old proteasomes in comparison to new proteasomes. We showed that proteins associated with the proteasome, posttranslational modifications of the proteasome, and subcellular localization of the proteasome change over time after proteasome biogenesis. By establishing a cell line in which we can discriminate new and old proteasomes, we further investigated the mechanism of proteasome turnover in a genome-wide siRNA screen and identified *CSNK2A2* as an important gene that is involved in proteasome turnover, possibly through phosphorylation of Rpn3.

An early study revealed that the half-life of proteasomes in rat hepatocytes was 12 to 15 days, whereas we found that the half-life in Rpn11-Flag MEFs was about 16 h (29). This conflict can be explained by the difference in growth rate between those cell lines. Although we found that the abundance of 3-day-old proteasomes was less than 5% of the total proteasomes and therefore characterized these as "old proteasomes" (Fig. 2A), 3 days postsynthesis may not be long enough to observe clear modifications. We acknowledge that what we observed from characterization of 3-day-old proteasomes could be the beginning or middle of the degradation process of the proteasome or modifications protecting proteasomes from proteolysis. In either case, we believe that our findings will contribute to a full understanding of the turnover mechanism of proteasomes.

Old proteasomes interacted with Txnl1, Usp14, and actin more than new proteasomes and were specifically phosphorylated in Rpn3 subunit at serine 6. We did not observe any significant change in the turnover rate of the proteasome by knockdown of either *TXNL1* or *USP14*, suggesting that association of Txnl1 and Usp14 with the proteasome has little or nothing to do with proteasome turnover (see Data Set S1 in the supplemental material). Usp14 has been reported to preferentially associate with proteasomes if they contain ubiquitinated proteins (47). This observation conflicts with the characteristic of old proteasomes. We assume that Usp14 could be recruited to old proteasomes through a different mechanism or that old proteasomes could make Usp14 less likely to dissociate. The relationship between actin and the proteasome is poorly understood, but their genetic interaction was reported in budding yeast (48). Although the mechanistic interplay is unclear, old proteasomes might be transported to a particular subcellular compartment along with the cytoskeleton, as suggested by previous reports (49, 50).

Although the total change in protein phosphorylation in Rpn11-Flag MEFs over 3 days was unknown, phosphorylation of Rpn3 was quite specific in that it was the only RP subunit that was clearly phosphorylated in old proteasomes. To investigate the role of phosphorylation of Rpn3, we tested putative phosphomimetic mutants of Rpn3 in which serine 6 was replaced with aspartic acid or glutamic acid (S6D or S6E, respectively) and a phosphor-null mutant of Rpn3 in which serine 6 was replaced with alanine (S6A). However, proteasomes incorporating these mutant Rpn3 did not show increased interactions with Txnl1 and Usp14 (data not shown). Also, overexpressed Rpn3 S6D and S6E fused with EGFP showed increased nuclear localization compared to wild-type or S6A mutant of Rpn3-EGFP (data not shown), which does not conform with the characteristics of old proteasomes (Fig. 5D and E). These results may suggest that phosphorylation of Rpn3 at serine 6 does not directly regulate the changes observed in old proteasomes. Alternatively, the result may reflect that Rpn3 S6D and S6E mutants do not accurately mimic phosphorylation of Rpn3, as often observed (51). The role of Rpn3 phosphorylation therefore remains elusive.

We note that the rate of phosphorylation of Rpn3 in 3-day-old proteasomes was not very high (Fig. 4A), which could be the reason why we did not observe a drastic effect

on proteasomal activities. However, although numerous phosphorylation sites of the proteasome have been reported, not all of them have validated biochemical effects (31–35), suggesting that phosphorylation of Rpn3 at serine 6 does not necessarily alter the activities of the proteasome. We presume that this phosphorylation site is recognized by unidentified factors that directly or indirectly trigger the characteristics of old proteasomes or regulate the stability of old proteasomes.

While CK2α' was found to affect the phosphorylation status of Rpn3, the detailed molecular mechanism of this phosphorylation is not understood at this point. We have tested *in vitro* kinase assay using recombinant proteins, but failed to detect direct phosphorylation of Rpn3 by CK2α'. Other proteins or a set of specific experimental conditions might be required for reconstitution of phosphorylation of Rpn3 *in vitro*. Although the direct kinase that phosphorylates Rpn3 at serine 6 is unknown, we presume that a kinase cascade involving CK2α' might be engaged in the turnover mechanism of the proteasome, considering that the proteasome is regulated by multiple phosphorylations (31–35). In addition to CK2α', casein kinase II has another catalytic subunit CK2α which is encoded by *CSNK2A1*. As knockdown of *CSNK2A1* did not delay the turnover of proteasomes in the primary screen (cf. Data Set S1), the roles of two catalytically active subunits of casein kinase II on the proteasome might not be redundant.

The subcellular localization of new and old proteasomes was different. Old proteasomes were mainly detected in cytoplasm, while new and total proteasomes were predominantly nuclear (Fig. 5D and E). The subcellular localization of the proteasome may be dependent on cell types, cell cycle, and stress conditions (52, 53). In particular, yeast proteasomes are localized in cytoplasm quiescent yeast cells (54). We therefore assume that being localized in cytoplasm might be important for the turnover mechanism of old proteasomes.

We then attempted to clarify the turnover mechanism of the proteasome by utilizing the cell lines in which we can discriminate between old and new proteasomes by pulse-chase HaloTag labeling. Since the proteasome is a complex of 33 subunits, the turnover of Rpn11 might not always be followed by other subunits. However, previous studies showed that almost all of the Rpn11 expressed in HeLa cells are incorporated into the 26S proteasome and that the half-lives of RP subunits and CP subunits are almost the same, respectively (28, 55). These reports suggest that the proteasome is not disassembled into each subunit when the proteasome is degraded and that the turnover of Rpn11 can at least represent that of an RP complex.

Considering that the half-life of proteasomes was almost the same with the doubling time of Rpn11-Flag MEFs (Fig. 2A and Fig. S2A) or Rpn11-Halo HeLa (Fig. 6E and Fig. S2B), we assume that the contribution of exponential decay to the degradation of old proteasomes might not be small. To test this possibility, we have compared the half-life of proteasomes with that of a stable protein Venus in the third screen. We were able to eliminate a few genes whose knockdown caused severe growth retardation which resulted in delayed exponential decay, such as *CKAP5* (microtubule polymerase) and *NUF2* (chromosome segregation). In other words, we were able to select genes whose knockdown delayed the turnover of proteasomes while having little effect on its exponential decay. These findings suggest that a process that regulates the turnover of proteasomes may exist.

Through siRNA screening, we did not identify particular pathways in which proteasomes are constitutively degraded, but there are five remaining screening hits that were not explored in this study. *ARCN* encodes the ∂ subunit of the coat protein I (COPI) complex which is required for Golgi-to-endoplasmic reticulum retrograde transport. Since COPI vesicle trafficking is known to be connected with actin dynamics (56), identification of this gene raised the possibility of regulation of old proteasomes by cytoskeleton dynamics. Similarly, *SORL1*, which encodes an endocytic receptor, could be engaged in the translocation of old proteasomes by intracellular trafficking system. Interestingly, genetic variation of *SORL1* has been identified to associate with Alzheimer's disease, which is related to impairment of the ubiquitin-proteasome system (57,

58), suggesting a relationship between aging of the proteasome and age-related diseases. *EPOR* and *NR1H2* encode the receptor of erythropoietin and oxysterol, respectively, which are unlikely to directly regulate turnover of the proteasome. However, both of these genes are expressed in most of the cultured cell lines, including HeLa cells (45). We assume that their unknown genetic interactions or functions may exist, since an erythropoietin-independent role of the erythropoietin receptor has been reported (59). *SAYSD1* is an uncharacterized gene, which may be a topic of future investigation.

Recently published papers reported that the proteasome is degraded by autophagy when cells are exposed to starvation or proteasome inhibition (24–27). However, we did not observe any delay in the turnover of proteasomes by knockdown of autophagy-related genes in the siRNA screen in which mammalian cells were cultured with sufficient nutrients (cf. Data Set S1). We do not preclude the possibility that autophagy plays a role in the constitutive degradation of the proteasome, but our data suggest that its contribution may be small. Thus, the degradation pathway of proteasomes under normal conditions still remains to be identified.

We focused on aging of the proteasome as a molecular complex and did not investigate its involvement in age-related disease. However, the connection between aging of the proteasome following synthesis and age-related diseases is potentially possible considering the importance of the turnover mechanism of the proteasome in protein quality control and the relationship between age-related diseases and impaired proteasome activities. While future studies on old proteasomes in aged tissues or animals will be necessary, we believe that our pioneering work should provide clues to the mechanism and the significance of proteasome turnover and its relationship to cellular and organismal senescence.

MATERIALS AND METHODS

Gene targeting of *Psmd14*. The targeting vector for Rpn11-Flag/EGFP knock-in was constructed by inserting 6×His-Flag and polyadenylation signal at the 3′ end of *Psmd14* (Rpn11) exon 12 with a PGK promoter-driven neomycin resistance gene cassette flanked by *FRT* sites. This sequence was flanked by *loxP* sites and followed by an additional exon 12 with EGFP coding sequence and polyadenylation signal fused to its 3′ end so that the expression of Flag tag was exchanged for EGFP tag by Cre recombinase. cDNA of EGFP was derived from pEGFP-N1 (Clontech Laboratories, Mountain View, CA). The targeting construct was linearized and electroporated into TT2 embryonic stem cells as described previously (60). For Southern blot analysis, genomic DNA was digested with KpnI and was hybridized with the probes shown in Fig. 1A. The genotypes of the knock-in mice were determined by PCR analysis of extracted genomic DNA using the following four primers: 5′-GATCAGGTTTAAGAGTTGTGCCTATGTAAG-3′, 5′-TAACTGTGAGCATTGGGAACGAAGA-3′, 5′-CATGCCTGCTATTGTCTTCCCAATCC-3′, and 5′-ACCATGTGATCGCGCTTCTCGTTGG-3′.

The 0.8-, 1.0-, and 1.5-kb fragments were amplified in the wild-type, Rpn11-Flag, and Rpn11-EGFP alleles, respectively. EIIa-Cre mice were purchased from the Jackson Laboratory (Bar Harbor, ME). All animal protocols were approved by the Institutional Animal Care Committee of Graduate School of Pharmaceutical Sciences, the University of Tokyo (approval no. M25-19) and carried out in accordance with the guidelines set by this committee. Mice were housed in pathogen-free facilities.

Cell culture and reagents. MEFs, HeLa cells, and HEK293T cells were cultured in Dulbecco modified Eagle medium (DMEM) supplemented with 10% (MEFs) or 5% (HeLa and HEK293T cells) fetal bovine serum (Thermo Fisher Scientific, Waltham, MA), 100 U/ml penicillin, and 100 μg/ml streptomycin at 37°C with 5% CO_2 incubation. Cre recombinase was expressed in *Psmd14*$^{Flag/+}$ ES cells via adenovirus or in Rpn11-Flag MEFs via retrovirus. Adenovirus expressing Cre recombinase was purified by using an Adeno-X Maxi purification kit (Clontech Laboratories). Vectors for control and Cre recombinase-expressing retrovirus (pCLNCX EGFP, pCLNCX NLS-Cre, and pMD.G/vsv-g) were kindly provided by Hiroshi Nishina (Tokyo Medical and Dental University) (61). The cDNAs encoding Rpn3 and CK2α' were isolated from HEK293T cells by RT-PCR using total RNA and subcloned into modified pIRES vectors (Clontech Laboratories). All constructs were confirmed by sequencing. Transfection of plasmids and siRNA was performed using Lipofectamine LTX and PLUS and Lipofectamine RNAiMAX (Thermo Fisher Scientific), respectively. The sequences of the dsRNAs were as follows: negative control, 5′-AUGUAUUGGCCUGUAUUAGUU-3′ and 5′-CUAAUACAGGCCAAUACAUUU-3′, and CSNK2A2, 5′-GGACAACUAUGACCAGCUUUU-3′ and 5′-AAGCUGGUCAUAGUUGUCCUU-3′.

Pulse-chase experiments. To measure the half-life of proteasomes in Rpn11-Flag MEFs, cells were metabolically labeled with [^{35}S]methionine for 24 h, washed twice with phosphate-buffered saline (PBS), and chased. 26S proteasomes purified from the cell lysates were subjected to SDS-PAGE and visualized by autoradiography. For HaloTag labeling, cells were cultured in the medium added with 100 nM Oregon green (OG), 10 nM tetramethylrhodamine (TMR), or 10 μM blocking ligand succinimidyl ester (O4) for 15 min and washed twice with PBS). Succinimidyl ester (O4) was incubated with 100 mM Tris-HCl (pH 8.0) for 60 min at 25°C before use. To generate HeLa cells stably expressing Tet-On-inducible Venus, HeLa

cells were transfected with pCMV-Tet3G (Clontech Laboratories) and selected with 0.8 mg/ml G418. The selected cells were further transfected with pTRE3G-IRES (Clontech Laboratories) encoding Venus and puromycin resistance gene, followed by 4 μg/ml puromycin selection.

Generation of Rpn11-Halo knock-in cells. Two CRISPR guide RNA (gRNA) sequences near the stop codon of human Rpn11 were chosen. Pairs of oligonucleotides for the site (GTAAACACTGGACAATATTTG for clone 1 and GTTCCTCCAAATGACGTTTG for clone 2) were annealed, phosphorylated, and ligated into the pX330 vector (Addgene, Cambridge, MA) (44). For homologous recombination, the targeting vector was constructed by inserting the HaloTag coding sequence and polyadenylation signal into the 3′ end of the last coding nucleotide in exon 12 of the human Rpn11 gene (*PSMD14*) with a PGK-puromycin resistance gene cassette. HeLa cells were transfected with the pX330 vector and the targeting vector and then selected with 4 μg/ml puromycin. The genotypes of puromycin-resistant colonies were determined by PCR analysis of extracted genomic DNA using the primers 5′-TGGTTCTGTTTTCTCTTTCC-3′ and 5′-CATTCCTTTAATGAAGCTACAGTAATACTCTCACC-3′.

Antibodies. The antibodies against Rpn1 to -3, Rpn6 to -8, Rpn10, Rpn13, Rpt1 to -6, α2, β3, Uch37, Usp14, Txnl1, HHR23b, and PA28γ were described previously (62–67). Polyclonal antibodies against Rpn5, Rpn9, Rpn11, EGFP, and HaloTag were raised in rabbits by using recombinant proteins of human Rpn5 (residues 1 to 161), human Rpn9 (full length), human Rpn11 (residues 171 to 287), EGFP (full length), and HaloTag (full length), respectively. The antibody against Rpn12 was raised by immunizing guinea pig with human Rpn12 (full length). The antibodies for ubiquitin (Z0458; DakoCytomation A/S, Glostrup, Denmark), Flag (F1804; Sigma-Aldrich, St. Louis, MO), actin (MAB1501R; Millipore, Billerica, MA), α-tubulin (sc-5286; Santa Cruz Biotechnology, Dallas, TX), and GAPDH (sc-32233; Santa Cruz) were purchased from the indicated manufacturers.

Generation of specific antibodies against serine 6 phosphorylated and unphosphorylated forms of Rpn3. Serine 6 phosphorylation-specific antibody against Rpn3 was generated by immunizing a rabbit with phosphorylated peptides (MKQEGpSARRRGC) conjugated with keyhole limpet hemocyanin, followed by affinity purification and removal of the antibodies that reacted with unphosphorylated peptides (MKQEGSARRRGC). Antibodies against unphosphorylated Rpn3 were raised in a similar way; serum samples from a rabbit immunized by unphosphorylated peptides were affinity purified with unphosphorylated peptides, and then the antibodies that reacted with phosphorylated peptides were removed.

Biochemical analysis. Cells were lysed with ice-cold buffer A (25 mM Tris-HCl [pH 7.5], 0.2% [vol/vol] NP-40, 1 mM dithiothreitol, 2 mM ATP, and 5 mM $MgCl_2$) and clarified by centrifugation at 20,000 $\times$ *g* for 10 min at 4°C. For phosphorylation assays, phosphatase inhibitor mix (5 mM NaF, 1 mM Na_3VO_4, 5 mM $Na_4P_2O_7$, and 10 mM β-glycerophosphate) was added to the buffer A. In the fractionation analysis, cells were lysed with buffer B (25 mM HEPES-NaOH [pH 7.5], 10 mM KCl, and 5 mM $MgCl_2$) containing 1 μg/ml digitonin (Nacalai Tesque, Kyoto, Japan) and centrifuged at 1,000 $\times$ *g* for 5 min at 4°C to generate supernatant (cytosolic fraction) and pellet. The pellet was dissolved with buffer B containing 1% (vol/vol) Triton X-100 and 1 U/ml benzonase (Novagen, Billerica, MA), followed by incubation on ice for 20 min, followed in turn by centrifugation at 5,000 $\times$ *g* for 5 min at 4°C to obtain a clarified nuclear fraction. For immunoprecipitation, anti-Flag M2–agarose and Flag peptide were purchased from Sigma, and COSMOGEL Ig-Accept protein G was purchased from Nacalai. For Western blotting, samples boiled with SDS sample buffer were subjected to SDS-PAGE, transferred to polyvinylidene fluoride membrane, incubated with Blocking One (Nacalai), and analyzed by immunoblotting. All images were taken with an LAS 4000 (GE Healthcare) for immunoblotting or a Typhoon FLA 9000 (GE Healthcare) for fluorescence imaging. Quantification of bands was performed using Fusion SL4 (M&S Instruments, Osaka, Japan) and ImageJ (National Institutes of Health, Bethesda, MD). A silver stain kit (299-58901; Wako, Saitama, Japan), an OxyBlot kit (S7150; Millipore), and Phos-tag acrylamide (AAL-107; Wako) were used according to the manufacturers' instructions.

Microscopy. Fluorescence images of knock-in mice were captured by M165 FC (Leica Microsystems, Wetzlar, Germany). Fixed tissues from the knock-in mice with 4% paraformaldehyde (PFA) were infused with 10 to 30% sucrose, embedded in OCT (Sakura Finetek, Tokyo, Japan), and then frozen. Sections (10 μm) were mounted on glass slides, fixed with 4% PFA for 20 min at room temperature, and permeabilized with 0.2% Triton X-100 in PBS. The permeabilized samples were incubated in blocking buffer (1% bovine serum albumin, 1% goat serum, 1% glycerol, and 0.2% [vol/vol] Triton X-100 in PBS) for 1 h at room temperature and subjected to immunostaining. For the secondary antibodies, Alexa Fluor and ProLong Diamond were purchased from Thermo Fisher Scientific. The images were obtained with a TCS SP8 (Leica).

Assay of proteasome activity and glycerol gradient centrifugation analysis. To measure the deubiquitinating activity, purified proteasomes in buffer A were incubated with ubiquitin–7-amido-4-methylcoumarin (LifeSensors, Malvern, PA) at 37°C for 10 min. The emitted fluorescence was measured by a 1420 ARVO MX (Perkin-Elmer, Waltham, MA [excitation, 355 nm; emission, 460]). Similarly, fluorescent peptide substrates (Peptide Institute, Osaka, Japan) were used to measure chymotrypsin-like activity by succinyl–Leu-Leu-Vl-Tyr–7-amido-4-methylcoumarin (Suc-LLVY-AMC), trypsin-like activity by *t*-butyloxycarbonyl–Leu-Arg-Arg (Boc-LRR)–AMC, and caspase-like activity by *N*-benzyloxycarbonyl–Leu-Leu-Glu (Z-LLE)–AMC, as described previously (42). Purification of recombinant ^{35}S-labeled ornithine decarboxylase (ODC) and ^{35}S-labeled polyubiquitinated cIAP1 protein was performed as described previously (7). Then, 10 μl of purified proteasomes was mixed with ^{35}S-labeled ODC in the presence of antizyme or with ^{35}S-labeled polyubiquitinated cIAP1 in 50 μl of reaction buffer (25 mM Tris-HCl [pH 7.5], 1 mM dithiothreitol, 2 mM ATP, and 5 mM $MgCl_2$), followed by incubation at 37°C for 20 min. The radioactivity of the trichloroacetic acid-soluble fraction was determined by scintillation counting. For glycerol gradient

centrifugation analysis, clarified cell lysates were subjected to 8 to 32% (vol/vol) linear glycerol gradient centrifugation (22 h, 83,000 × *g*) and separated into 32 fractions, followed by measurement of peptidase activity of each fraction as described previously (7).

LC-MS/MS analysis of Rpn3. Identification of the phosphorylation site of Rpn3 was performed as described in previous reports (68, 69). Coomassie brilliant blue (CBB)-stained bands corresponding to Rpn3 were subjected to in-gel trypsin digestion and analyzed with Q-Exactive (Thermo Fisher Scientific). Mass spectrometry spectra were analyzed using a Protein Discoverer (Thermo Fisher Scientific). The fragmentation spectra were searched against the UniProt database with the MASCOT search engine. Multiple alignment was carried out by Clustal Omega (1.2.1).

siRNA library and screening strategy. The genome-wide siRNA library (Human Genome [G-005005], Human Druggable Subsets [G-004675], and Human Drug Target [G-004655]; Thermo Fisher Scientific), covering siRNA targeting 18,151 genes in total with pools of four sequences per target gene, was dissolved in UltraPure distilled water (Thermo Fisher Scientific), and 2.5 μl of 1 μM siRNA solution was dispensed into 384-well μClear cell culture microplates (781090; Greiner, Kremsmuenster, Austria). Before plating cells on the microplates, the siRNA in the plates was mixed with 0.1 μl of Lipofectamine RNAiMAX in 10 μl of DMEM. Rpn11-Halo knock-in HeLa cells (clone 2) treated with OG and the blocking ligand in 40 μl of culture medium were plated on the assay plate (1,500 cells per plate) and cultured. After 64 h, 10 μl of TMR solution in culture medium was added, and then the cells were fixed by adding 10 μl of 10% PFA (final concentration, 1.6%) for 20 min at room temperature. The PFA was removed, and the plate was washed with 80 μl of 25 mM Tris-HCl (pH 8.0). To stain nuclei, each well was filled with 40 μl of buffer containing DAPI (25 mM Tris-HCl [pH 8.0], 2% [wt/vol] triethylenediamine, and 500 ng/ml DAPI).

The cell images were obtained with CellInsight NXT (Thermo Fisher Scientific). The cells were recognized by DAPI fluorescence, and the fluorescence intensities of the OG and TMR were quantified. To adjust positional effects, raw data were subjected to median polish using statistical software R and B score of each targeted gene was calculated as described previously (70, 71).

In the second screen, individual siRNAs for the hit wells in the primary screen were purchased from GE Dharmacon (Lafayette, CO). Rpn11-Halo knock-in cells were analyzed in the same way with the primary screen, except that labeling of newly synthesized Rpn11-Halo just before PFA fixation was omitted. To measure the turnover of Venus protein, HeLa cells stably expressing Tet-On-inducible Venus were cultured with 100 ng/ml doxycycline for 8 h, washed twice with PBS, and plated on siRNA assay plates. In the flow cytometry analysis, Rpn11-Halo knock-in cells cultured in 96-well plates were treated with HaloTag ligands in the same way with the primary screen. After TMR labeling, the cells were harvested by trypsinization and subjected to measurement of fluorescence intensities by Attune NxT (Thermo Fisher Scientific).

RNA isolation and RT-PCR. Total RNAs were isolated with High Pure RNA isolation kit (Roche, Basel, Switzerland) and reverse transcribed to cDNA using ReverTra Ace (TOYOBO, Osaka, Japan). PCR primers for RT-PCR are as follows: *ACTB*, 5′-CCAACCGCGAGAAGATGA-3′ and 5′-CCAGAGGCGTACAGGGATAG-3′; *CSNK2A2*, 5′-CCATGGAGCACCCATACTTC-3′ and 5′-CACAGCATTGTCTGCACAAG-3′; *Actb*, 5′-CTAAGGCCA ACCGTGAAAAG-3′ and 5′-ACCAGAGGCATACAGGGACA-3′; and *Csnk2a2*, 5′-CCATGGAGCACCCATATTT C-3′ and 5′-CACGGTGTTCTCAGCACAAG-3′.

Statistical analysis. Statistical significance was calculated by using an unpaired two-tailed *t* test or a one-sample *t* test.

SUPPLEMENTAL MATERIAL

Supplemental material for this article may be found at https://doi.org/10.1128/MCB.00426-18.

SUPPLEMENTAL FILE 1, PDF file, 7.3 MB.

SUPPLEMENTAL FILE 2, XLSX file, 1.2 MB.

ACKNOWLEDGMENTS

We thank Hidenori Ichijo and Isao Naguro for advice on the generation of phosphorylation-specific antibodies and the siRNA screen. We are also grateful to Hiroshi Nishina for Cre recombinase expression vectors.

This study was supported by JSPS KAKENHI grants JP25221102 and JP26111704 and the AMED-CREST from the Japan Agency for Medical Research and Development (JP18gm1110003).

REFERENCES

1. Glickman MH, Ciechanover A. 2002. The ubiquitin-proteasome proteolytic pathway: destruction for the sake of construction. Physiol Rev 82:373–428. https://doi.org/10.1152/physrev.00027.2001.
2. Finley D. 2009. Recognition and processing of ubiquitin-protein conjugates by the proteasome. Annu Rev Biochem 78:477–513. https://doi.org/10.1146/annurev.biochem.78.081507.101607.
3. Murata S, Yashiroda H, Tanaka K. 2009. Molecular mechanisms of proteasome assembly. Nat Rev Mol Cell Biol 10:104–115. https://doi.org/10.1038/nrm2630.
4. Hirano Y, Hendil KB, Yashiroda H, Iemura S, Nagane R, Hioki Y, Natsume T, Tanaka K, Murata S. 2005. A heterodimeric complex that promotes the assembly of mammalian 20S proteasomes. Nature 437:1381–1385. https://doi.org/10.1038/nature04106.
5. Hirano Y, Hayashi H, Iemura S-I, Hendil KB, Niwa S-I, Kishimoto T,

Kasahara M, Natsume T, Tanaka K, Murata S. 2006. Cooperation of multiple chaperones required for the assembly of mammalian 20S proteasomes. Mol Cell 24:977–984. https://doi.org/10.1016/j.molcel.2006.11.015.
6. Borodovsky A, Kessler BM, Casagrande R, Overkleeft HS, Wilkinson KD, Ploegh HL. 2001. A novel active site-directed probe specific for deubiquitylating enzymes reveals proteasome association of USP14. EMBO J 20:5187–5196. https://doi.org/10.1093/emboj/20.18.5187.
7. Hamazaki J, Iemura S-I, Natsume T, Yashiroda H, Tanaka K, Murata S. 2006. A novel proteasome interacting protein recruits the deubiquitinating enzyme UCH37 to 26S proteasomes. EMBO J 25:4524–4536. https://doi.org/10.1038/sj.emboj.7601338.
8. Hiyama H, Yokoi M, Masutani C, Sugasawa K, Maekawa T, Tanaka K, Hoeijmakers JHJ, Hanaoka F. 1999. Interaction of hHR23 with S5a. J Biol Chem 274:28019–28025. https://doi.org/10.1074/jbc.274.39.28019.
9. Mah AL, Perry G, Smith MA, Monteiro MJ. 2000. Identification of ubiquilin, a novel presenilin interactor that increases presenilin protein accumulation. J Cell Physiol 151:847–862.
10. Andersen KM, Madsen L, Prag S, Johnsen AH, Semple CA, Hendil KB, Hartmann-Petersen R. 2009. Thioredoxin Txnl1/TRP32 is a redox-active cofactor of the 26 S proteasome. J Biol Chem 284:15246–15254. https://doi.org/10.1074/jbc.M900016200.
11. Wiseman RL, Chin K-T, Haynes CM, Stanhill A, Xu C-F, Roguev A, Krogan NJ, Neubert TA, Ron D. 2009. Thioredoxin-related protein 32 is an arsenite-regulated thiol reductase of the proteasome 19S particle. J Biol Chem 284:15233–15245. https://doi.org/10.1074/jbc.M109.002121.
12. Ravid T, Hochstrasser M. 2008. Diversity of degradation signals in the ubiquitin-proteasome system. Nat Rev Mol Cell Biol 9:679–690. https://doi.org/10.1038/nrm2468.
13. Schwartz AL, Ciechanover A. 2009. Targeting proteins for destruction by the ubiquitin system: implications for human pathobiology. Annu Rev Pharmacol Toxicol 49:73–96. https://doi.org/10.1146/annurev.pharmtox.051208.165340.
14. Schmidt M, Finley D. 2014. Regulation of proteasome activity in health and disease. Biochim Biophys Acta 1843:13–25. https://doi.org/10.1016/j.bbamcr.2013.08.012.
15. Saez I, Vilchez D. 2014. The mechanistic links between proteasome activity, aging and age-related diseases. Curr Genomics 15:38–51. https://doi.org/10.2174/1389202915011403061133 44.
16. Dennissen FJA, Kholod N, van Leeuwen FW. 2012. The ubiquitin proteasome system in neurodegenerative diseases: culprit, accomplice or victim? Prog Neurobiol 96:190–207. https://doi.org/10.1016/j.pneurobio.2012.01.003.
17. Agarwal AK, Xing C, DeMartino GN, Mizrachi D, Hernandez MD, Sousa AB, Martínez de Villarreal L, dos Santos HG, Garg A. 2010. PSMB8 encoding the β5i proteasome subunit is mutated in joint contractures, muscle atrophy, microcytic anemia, and panniculitis-induced lipodystrophy syndrome. Am J Hum Genet 87:866–872. https://doi.org/10.1016/j.ajhg.2010.10.031.
18. Arima K, Kinoshita A, Mishima H, Kanazawa N, Kaneko T, Mizushima T, Ichinose K, Nakamura H, Tsujino A, Kawakami A, Matsunaka M, Kasagi S, Kawano S, Kumagai S, Ohmura K, Mimori T, Hirano M, Ueno S, Tanaka K, Tanaka M, Toyoshima I, Sugino H, Yamakawa A, Tanaka K, Niikawa N, Furukawa F, Murata S, Eguchi K, Ida H, Yoshiura K-I. 2011. Proteasome assembly defect due to a proteasome subunit beta type 8 (PSMB8) mutation causes the autoinflammatory disorder, Nakajo-Nishimura syndrome. Proc Natl Acad Sci U S A 108:14914–14919. https://doi.org/10.1073/pnas.1106015108.
19. Kitamura A, Maekawa Y, Uehara H, Izumi K, Kawachi I, Nishizawa M, Toyoshima Y, Takahashi H, Standley DM, Tanaka K, Hamazaki J, Murata S, Obara K, Toyoshima I, Yasutomo K. 2011. A mutation in the immunoproteasome subunit PSMB8 causes autoinflammation and lipodystrophy in humans. J Clin Invest 121:4150–4160. https://doi.org/10.1172/JCI58414.
20. Liu Y, Ramot Y, Torrelo A, Paller AS, Si N, Babay S, Kim PW, Sheikh A, Lee C-CR, Chen Y, Vera A, Zhang X, Goldbach-Mansky R, Zlotogorski A. 2012. Mutations in proteasome subunit β type 8 cause chronic atypical neutrophilic dermatosis with lipodystrophy and elevated temperature with evidence of genetic and phenotypic heterogeneity. Arthritis Rheum 64:895–907. https://doi.org/10.1002/art.33368.
21. Vilchez D, Morantte I, Liu Z, Douglas PM, Merkwirth C, Rodrigues APC, Manning G, Dillin A. 2012. RPN-6 determines *Caenorhabditis elegans* longevity under proteotoxic stress conditions. Nature 489:263–268. https://doi.org/10.1038/nature11315.
22. Vilchez D, Boyer L, Morantte I, Lutz M, Merkwirth C, Joyce D, Spencer B, Page L, Masliah E, Berggren WT, Gage FH, Dillin A. 2012. Increased proteasome activity in human embryonic stem cells is regulated by PSMD11. Nature 489:304–308. https://doi.org/10.1038/nature11468.
23. Tonoki A, Kuranaga E, Tomioka T, Hamazaki J, Murata S, Tanaka K, Miura M. 2009. Genetic evidence linking age-dependent attenuation of the 26S proteasome with the aging process. Mol Cell Biol 29:1095–1106. https://doi.org/10.1128/MCB.01227-08.
24. Marshall RS, Li F, Gemperline DC, Book AJ, Vierstra RD. 2015. Autophagic degradation of the 26S proteasome is mediated by the dual ATG8/ubiquitin receptor RPN10 in *Arabidopsis*. Mol Cell 58:1053–1066. https://doi.org/10.1016/j.molcel.2015.04.023.
25. Waite KA, De-La Mota-Peynado A, Vontz G, Roelofs J. 2016. Starvation induces proteasome autophagy with different pathways for core and regulatory particles. J Biol Chem 291:3239–3253. https://doi.org/10.1074/jbc.M115.699124.
26. Marshall RS, McLoughlin F, Vierstra RD. 2016. Autophagic turnover of inactive 26S proteasomes in yeast is directed by the ubiquitin receptor Cue5 and the Hsp42 chaperone. Cell Rep 16:1717–1732. https://doi.org/10.1016/j.celrep.2016.07.015.
27. Cohen-Kaplan V, Livneh I, Avni N, Fabre B, Ziv T, Kwon YT, Ciechanover A. 2016. p62- and ubiquitin-dependent stress-induced autophagy of the mammalian 26S proteasome. Proc Natl Acad Sci U S A 113:E7490–E7499. https://doi.org/10.1073/pnas.1615455113.
28. Schwanhäusser B, Busse D, Li N, Dittmar G, Schuchhardt J, Wolf J, Chen W, Selbach M. 2011. Global quantification of mammalian gene expression control. Nature 473:337–342. https://doi.org/10.1038/nature10098.
29. Tanaka K, Ichihara A. 1989. Half-life of proteasomes (multiprotease complexes) in rat liver. Biochem Biophys Res Commun 159:1309–1315. https://doi.org/10.1016/0006-291X(89)92253-5.
30. Lakso M, Pichel JG, Gorman JR, Sauer B, Okamoto Y, Lee E, Alt FW, Westphal H. 1996. Efficient *in vivo* manipulation of mouse genomic sequences at the zygote stage. Proc Natl Acad Sci U S A 93:5860–5865. https://doi.org/10.1073/pnas.93.12.5860.
31. Hirano H, Kimura Y, Kimura A. 2016. Biological significance of co- and posttranslational modifications of the yeast 26S proteasome. J Proteomics 134:37–46. https://doi.org/10.1016/j.jprot.2015.11.016.
32. Aiken CT, Kaake RM, Wang X, Huang L. 2011. Oxidative stress-mediated regulation of proteasome complexes. Mol Cell Proteomics 10:R110.006924. https://doi.org/10.1074/mcp.M110.006924.
33. Cui Z, Scruggs SB, Gilda JE, Ping P, Gomes AV. 2014. Regulation of cardiac proteasomes by ubiquitination, SUMOylation, and beyond. J Mol Cell Cardiol 71:32–42. https://doi.org/10.1016/j.yjmcc.2013.10.008.
34. Collins GA, Goldberg AL. 2017. The logic of the 26S proteasome. Cell 169:792–806. https://doi.org/10.1016/j.cell.2017.04.023.
35. Guo X, Huang X, Chen MJ. 2017. Reversible phosphorylation of the 26S proteasome. Protein Cell 8:255–272. https://doi.org/10.1007/s13238-017-0382-x.
36. Sell DR, Strauch CM, Shen W, Monnier VM. 2007. 2-aminoadipic acid is a marker of protein carbonyl oxidation in the aging human skin: effects of diabetes, renal failure and sepsis. Biochem J 404:269–277. https://doi.org/10.1042/BJ20061645.
37. Kinoshita E, Kinoshita-Kikuta E, Koike T. 2009. Separation and detection of large phosphoproteins using Phos-tag SDS-PAGE. Nat Protoc 4:1513–1521. https://doi.org/10.1038/nprot.2009.154.
38. Schweitzer A, Aufderheide A, Rudack T, Beck F, Pfeifer G, Plitzko JM, Sakata E, Schulten K, Förster F, Baumeister W. 2016. Structure of the human 26S proteasome at a resolution of 3.9 Å. Proc Natl Acad Sci U S A 113:7816–7821. https://doi.org/10.1073/pnas.1608050113.
39. Lander GC, Estrin E, Matyskiela ME, Bashore C, Nogales E, Martin A. 2012. Complete subunit architecture of the proteasome regulatory particle. Nature 482:186–191. https://doi.org/10.1038/nature10774.
40. Murakami Y, Matsufuji S, Kameji T, Hayashi S, Igarashi K, Tamura T, Tanaka K, Ichihara A. 1992. Ornithine decarboxylase is degraded by the 26S proteasome without ubiquitination. Nature 360:597–599. https://doi.org/10.1038/360597a0.
41. Yang Y, Fang S, Jensen JP, Weissman AM, Ashwell JD. 2000. Ubiquitin protein ligase activity of IAPs and their degradation in proteasomes in response to apoptotic stimuli. Science 288:874–877. https://doi.org/10.1126/science.288.5467.874.
42. Murata S, Sasaki K, Kishimoto T, Niwa S-I, Hayashi H, Takahama Y, Tanaka K. 2007. Regulation of $CD8^+$ T cell development by thymus-specific proteasomes. Science 316:1349–1353. https://doi.org/10.1126/science.1141915.
43. Los GV, Encell LP, McDougall MG, Hartzell DD, Karassina N, Zimprich C,

Wood MG, Learish R, Ohana RF, Urh M, Simpson D, Mendez J, Zimmerman K, Otto P, Vidugiris G, Zhu J, Darzins A, Klaubert DH, Bulleit RF, Wood KV. 2008. HaloTag: a novel protein labeling technology for cell imaging and protein analysis. ACS Chem Biol 3:373–382. https://doi.org/10.1021/cb800025k.
44. Cong L, Ran FA, Cox D, Lin S, Barretto R, Habib N, Hsu PD, Wu X, Jiang W, Marraffini LA, Zhang F. 2013. Multiplex genome engineering using CRISPR/Cas systems. Science 339:819–823. https://doi.org/10.1126/science.1231143.
45. Thul PJ, Åkesson L, Wiking M, Mahdessian D, Geladaki A, Ait Blal H, Alm T, Asplund A, Björk L, Breckels LM, Bäckström A, Danielsson F, Fagerberg L, Fall J, Gatto L, Gnann C, Hober S, Hjelmare M, Johansson F, Lee S, Lindskog C, Mulder J, Mulvey CM, Nilsson P, Oksvold P, Rockberg J, Schutten R, Schwenk JM, Sivertsson Å, Sjöstedt E, Skogs M, Stadler C, Sullivan DP, Tegel H, Winsnes C, Zhang C, Zwahlen M, Mardinoglu A, Pontén F, von Feilitzen K, Lilley KS, Uhlén M, Lundberg E. 2017. A subcellular map of the human proteome. Science 356:eaal3321. https://doi.org/10.1126/science.aal3321.
46. Litchfield DW. 2003. Protein kinase CK2: structure, regulation and role in cellular decisions of life and death. Biochem J 369:1–15. https://doi.org/10.1042/bj20021469.
47. Kuo C-L, Goldberg AL. 2017. Ubiquitinated proteins promote the association of proteasomes with the deubiquitinating enzyme Usp14 and the ubiquitin ligase Ube3c. Proc Natl Acad Sci U S A 114:E3404–E3413. https://doi.org/10.1073/pnas.1701734114.
48. Haarer B, Aggeli D, Viggiano S, Burke DJ, Amberg DC. 2011. Novel interactions between actin and the proteasome revealed by complex haploinsufficiency. PLoS Genet 7:e1002288. https://doi.org/10.1371/journal.pgen.1002288.
49. Gorbea C, Pratt G, Ustrell V, Bell R, Sahasrabudhe S, Hughes RE, Rechsteiner M. 2010. A protein interaction network for Ecm29 links the 26 S proteasome to molecular motors and endosomal components. J Biol Chem 285:31616–31633. https://doi.org/10.1074/jbc.M110.154120.
50. Hsu M-T, Guo C-L, Liou AY, Chang T-Y, Ng M-C, Florea BI, Overkleeft HS, Wu Y-L, Liao J-C, Cheng P-L. 2015. Stage-dependent axon transport of proteasomes contributes to axon development. Dev Cell 35:418–431. https://doi.org/10.1016/j.devcel.2015.10.018.
51. Dephoure N, Gould KL, Gygi SP, Kellogg DR. 2013. Mapping and analysis of phosphorylation sites: a quick guide for cell biologists. Mol Biol Cell 24:535–542. https://doi.org/10.1091/mbc.e12-09-0677.
52. Wójcik C, DeMartino GN. 2003. Intracellular localization of proteasomes. Int J Biochem Cell Biol 35:579–589. https://doi.org/10.1016/S1357-2725(02)00380-1.
53. Chowdhury M, Enenkel C. 2015. Intracellular dynamics of the ubiquitin-proteasome system. F1000Res 4:367. https://doi.org/10.12688/f1000research.6835.2.
54. Laporte D, Salin B, Daignan-Fornier B, Sagot I. 2008. Reversible cytoplasmic localization of the proteasome in quiescent yeast cells. J Cell Physiol 181:737–745. https://doi.org/10.1083/jcb.200711154.
55. Hendil KB, Kriegenburg F, Tanaka K, Murata S, Lauridsen A-MB, Johnsen AH, Hartmann-Petersen R. 2009. The 20S proteasome as an assembly platform for the 19S regulatory complex. J Mol Biol 394:320–328. https://doi.org/10.1016/j.jmb.2009.09.038.
56. Gurel PS, Hatch AL, Higgs HN. 2014. Connecting the cytoskeleton to the endoplasmic reticulum and Golgi. Curr Biol 24:R660–R672. https://doi.org/10.1016/j.cub.2014.05.033.
57. Sulistio YA, Heese K. 2016. The ubiquitin-proteasome system and molecular chaperone deregulation in Alzheimer's disease. Mol Neurobiol 53:905–931. https://doi.org/10.1007/s12035-014-9063-4.
58. Yin R-H, Yu J-T, Tan L. 2015. The role of SORL1 in Alzheimer's disease. Mol Neurobiol 51:909–918. https://doi.org/10.1007/s12035-014-8742-5.
59. Reinbothe S, Larsson A-M, Vaapil M, Wigerup C, Sun J, Jögi A, Neumann D, Rönnstrand L, Påhlman S. 2014. EPO-independent functional EPO receptor in breast cancer enhances estrogen receptor activity and promotes cell proliferation. Biochem Biophys Res Commun 445:163–169. https://doi.org/10.1016/j.bbrc.2014.01.165.
60. Murata S, Kawahara H, Tohma S, Yamamoto K, Kasahara M, Nabeshima Y, Tanaka K, Chiba T. 1999. Growth retardation in mice lacking the proteasome activator PA28γ. J Biol Chem 274:38211–38215. https://doi.org/10.1074/jbc.274.53.38211.
61. Uchida Y, Osaki T, Yamasaki T, Shimomura T, Hata S, Horikawa K, Shibata S, Todo T, Hirayama J, Nishina H. 2012. Involvement of stress kinase mitogen-activated protein kinase kinase 7 in regulation of mammalian circadian clock. J Biol Chem 287:8318–8326. https://doi.org/10.1074/jbc.M111.308908.
62. Kaneko T, Hamazaki J, Iemura S-I, Sasaki K, Furuyama K, Natsume T, Tanaka K, Murata S. 2009. Assembly pathway of the mammalian proteasome base subcomplex is mediated by multiple specific chaperones. Cell 137:914–925. https://doi.org/10.1016/j.cell.2009.05.008.
63. Uechi H, Hamazaki J, Murata S. 2014. Characterization of the testis-specific proteasome subunit α4s in mammals. J Biol Chem 289:12365–12374. https://doi.org/10.1074/jbc.M114.558866.
64. Hamazaki J, Hirayama S, Murata S. 2015. Redundant roles of Rpn10 and Rpn13 in recognition of ubiquitinated proteins and cellular homeostasis. PLoS Genet 11:e1005401. https://doi.org/10.1371/journal.pgen.1005401.
65. Hamazaki J, Sasaki K, Kawahara H, Hisanaga S-I, Tanaka K, Murata S. 2007. Rpn10-mediated degradation of ubiquitinated proteins is essential for mouse development. Mol Cell Biol 27:6629–6638. https://doi.org/10.1128/MCB.00509-07.
66. Moriishi K, Okabayashi T, Nakai K, Moriya K, Koike K, Murata S, Chiba T, Tanaka K, Suzuki R, Suzuki T, Miyamura T, Matsuura Y. 2003. Proteasome activator PA28-dependent nuclear retention and degradation of hepatitis C virus core protein. J Virol 77:10237–10249. https://doi.org/10.1128/JVI.77.19.10237-10249.2003.
67. Uechi H, Kuranaga E, Iriki T, Takano K, Hirayama S, Miura M, Hamazaki J, Murata S. 2017. Ubiquitin-binding protein CG5445 suppresses aggregation and cytotoxicity of amyotrophic lateral sclerosis-linked TDP-43 in *Drosophila*. Mol Cell Biol 38:e00195-17. https://doi.org/10.1128/MCB.00195-17.
68. Tsuchiya H, Tanaka K, Saeki Y. 2013. The parallel reaction monitoring method contributes to a highly sensitive polyubiquitin chain quantification. Biochem Biophys Res Commun 436:223–229. https://doi.org/10.1016/j.bbrc.2013.05.080.
69. Koyano F, Okatsu K, Kosako H, Tamura Y, Go E, Kimura M, Kimura Y, Tsuchiya H, Yoshihara H, Hirokawa T, Endo T, Fon EA, Trempe J-F, Saeki Y, Tanaka K, Matsuda N. 2014. Ubiquitin is phosphorylated by PINK1 to activate Parkin. Nature 510:162–166. https://doi.org/10.1038/nature13392.
70. Brideau C, Gunter B, Pikounis B, Liaw A. 2003. Improved statistical methods for hit selection in high-throughput screening. J Biomol Screen 8:634–647. https://doi.org/10.1177/1087057103258285.
71. Koizumi S, Irie T, Hirayama S, Sakurai Y, Yashiroda H, Naguro I, Ichijo H, Hamazaki J, Murata S. 2016. The aspartyl protease DDI2 activates Nrf1 to compensate for proteasome dysfunction. Elife 5:e18357. https://doi.org/10.7554/eLife.18357.